Reviews

Lithium Lanthanum Titanates: A Review

S. Stramare,† V. Thangadurai,* and W. Weppner

Chair for Sensors and Solid State Ionics, Faculty of Engineering, Christian-Albrechts-University of Kiel, Kaiserstr. 2, D-24143 Kiel, Germany

Received March 14, 2003. Revised Manuscript Received July 22, 2003

To date, the highest bulk lithium ion-conducting solid electrolyte is the perovskite (ABO_3)-type lithium lanthanum titanate (LLT) $Li_{3x}La_{(2/3)-x}\square_{(1/3)-2x}TiO_3$ ($0 < x < 0.16$) and its related structure materials. The $x \approx 0.1$ member exhibits conductivity of 1×10^{-3} S/cm at room temperature with an activation energy of 0.40 eV. The conductivity is comparable to that of commonly used polymer/liquid electrolytes. The ionic conductivity of LLT mainly depends on the size of the A-site ion cation (e.g., La or rare earth, alkali or alkaline earth), lithium and vacancy concentration, and the nature of the B−O bond. For example, replacement of La by other rare earth elements with smaller ionic radii than that of La decreases the lithium ion conductivity, while partial substitution of La by Sr (larger ionic radii than that of La) slightly increases the lithium ion conductivity. The high lithium ion conductivity of LLT is considered to be due to the large concentration of A-site vacancies, and the motion of lithium by a vacancy mechanism through the wide square planar bottleneck between the A sites. It is considered that BO_6/TiO_6 octahedra tilting facilitate the lithium ion mobility in the perovskite structure. The actual mechanism of lithium ion conduction is not yet clearly understood. In this paper, we review the structural properties, electrical conductivity, and electrochemical characterization of LLT and its related materials.

1. Introduction

At present, lithium ion secondary battery developments are mainly based on $LiCoO_2$ as a cathode (positive electrode), lithium ion-conducting organic polymer as an electrolyte ($LiPF_6$ dissolved in poly(ethylene oxide) (PEO)), and Li metal or graphite as an anode (negative electrode). The formation of a solid electrolyte interface (SEI) at the anode leads to a large irreversible capacity loss during the discharge cycles. A further major concern is the safety aspect of liquid and common polymeric electrolytes. The liquid-free batteries show some advantages over the currently commercialized ones. These include thermal stability, absence of leakage and pollution, resistance to shocks and vibrations, and large electrochemical windows of application, thanks to the use of high-voltage (~5.5 V/Li) cathode materials. Furthermore, the development in microelectronic and information technologies requires the search for a new generation of energy sources, among which a considerable interest has been given to the all-solid-state lithium batteries. The main impediment is finding an appropriate solid electrolyte that has a reasonably high lithium ionic conductivity and a good chemical stability in contact with both electrodes, especially with metallic lithium or LiAl alloy anode.[1,2]

A wide variety of metal oxides are known to exhibit high bulk lithium ion conductivity. Using temperature as scale, they can be divided mainly into two groups: (i) high-temperature ionic conductors, for example, Li_2SO_4,[3] Li_4SiO_4,[4] and $Li_{14}ZnGe_4O_{16}$ (Lithium Super Ionic Conductor, LISICON)[5] and (ii) low-temperature ionic conductors, for example, γ-$Li_{3.6}Ge_{0.6}V_{0.4}O_4$,[6] Li_3N,[7,8] Li-β-alumina,[9] $Li_{1+x}Ti_{2-x}M_x(PO_4)_3$ (M = Al, Sc, Y, La),[10] and $Li_{0.34}La_{0.5}TiO_{2.94}$.[11] They can also be classified into four groups according to the type of compounds: (i) lithium oxyacid salts, for example, Li_2SO_4 and Li_4SiO_4; (ii) γ -Li_3PO_4 solid solutions, for example, LISICON and γ-$Li_{3.6}Ge_{0.6}V_{0.4}O_4$; (iii) NASICON-structured $Li_{1+x}Ti_{2-x}M_x(PO_4)_3$ (M = Al, Ga, In, Sc), and (iv) Li ion-conducting *A*-site *d*eficient *p*erovskite solid *s*olution (Li-ADPESS).

To date, the fastest lithium ion-conducting solid electrolytes known are the perovskite-type (ABO_3) oxide, with A = Li, La and B = Ti, lithium lanthanum titanate (LLT) $Li_{3x}La_{(2/3)-x}\square_{(1/3)-2x}TiO_3$,[11,12] and its structurally related materials.[12−26] This paper aims at giving a comprehensive review of the available information about LLT and its related materials (A site, B site, or both substituted LLT), with special focus on composition−structure−ionic conductivity property.

2. General Considerations

Historically, perovskite-type alkaline-earth titanates ($ATiO_3$, A = Ca, Sr, Ba) aroused much interest due to their functional properties, for example, dielectricity and

* To whom correspondence should be addressed. E-mail: vt@tf.uni.kiel.de. Phone: 0049 431 880 6210. Fax: 0049 431 880 6203.
† Nanogate Technologies GmbH, Gewerbepark Eschbergerweg, D-66121 Saarbrücken, Germany.

10.1021/cm0300516 CCC: $25.00
Published on Web 09/23/2003

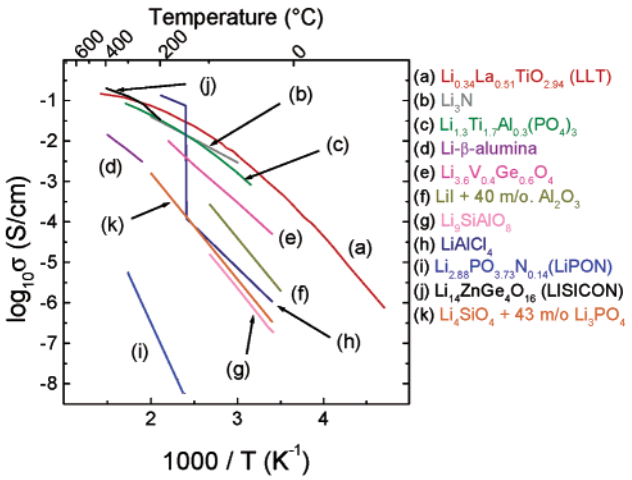

Figure 1. Arrhenius plots of electrical conductivity of perovskite-type lithium lanthanum titatate $Li_{0.34}La_{0.51}TiO_{2.94}$,[16] along with several well-known solid lithium ion conductors. The sharp increase in $LiAlCl_4$ is due to melting.

ferroelectricity, which arise from the displacement of Ti atoms toward one of the octahedrally coordinated oxygen atoms along the *c*-axis.[27a] Brous et al.[27b] reported for the first time the synthesis of cubic $Li_{0.5}La_{0.5}TiO_3$ by the replacement of A-site alkaline earth ions in $ATiO_3$ with a trivalent rare earth La ion and monovalent ions (Li, Na, K). Some years later, Patil and Chincholkar[28,29] confirmed this result and extended their investigation in which the La was replaced by other rare earth ions. After these structural studies, the dielectric properties of these perovskite-type titanates were considered by Varaprasad et al.,[30] who found the hysteresis and the dielectric anomaly peak at 67 °C in $Li_{0.5}La_{0.5}TiO_3$. On the basis of their results, they concluded that $Li_{0.5}La_{0.5}TiO_3$ exhibits both ferroelectric and antiferroelectric ordering. They and Kochergina et al.[31] assigned the structure of $Li_{0.5}La_{0.5}TiO_3$ to that of tetragonal tungsten bronze-type.[31b] Increase of the capacitance with increasing temperature, large dielectric loss, and dielectric relaxation were observed from Inaguma et al.,[11] who considered these phenomena due to Li-ion motion.

Indeed, the first studies on the conducting behavior and on the stoichiometric range of stability of LLT were reported by Belous et al.[14] They reported that oxides with nominal composition $Li_{3x}La_{(2/3)-x}\square_{(1/3)-2x}TiO_3$ show a perovskite-like structure for x in the range $0.04 < x < 0.17$, recognizing that the lanthanum ions, larger in ionic size, are the main contributors to the stabilization of the perovskite-type structure and that the lithium ions are the charge carriers responsible for their high electrical conductivity.[14]

However, the work of Inaguma et al.[11] is referred to as the first study on the ionic conductivity of LLT since they reported a bulk lithium ion conductivity of 1×10^{-3} S/cm at room temperature (RT). LLT has attracted the interest of many research groups around the world because of its possible potential application as solid electrolyte in various electrochemical devices, for example, all-solid-state lithium-ion batteries, sensors, and electrochromic displays. Figure 1 shows the Arrhenius plots for ionic conductivity of LLT together with well-known solid lithium ion conductors. Since 1993, the influence of the composition, partial substitution or total substitution of La and Ti with other metal ions, effect of pressure, and sintering conditions on their crystal structure, conductivity, electrochemical properties, and the mechanism for lithium ion conduction have been widely investigated.[12,19−26,32−100]

3. Synthesis of LLT and Related Materials

LLTs and related compounds have been synthesized mainly by three methods: (i) solid-state reaction, (ii) sol−gel synthesis,[49] and (iii) floating zone.[48,85] Among them, solid-state reactions are commonly used, allowing the production of relatively large quantities of bulk material. Sol−gel synthesis coupled with dip coating was introduced to prepare thin films of LLT for applying these materials in the solid-state devices.[49] A floating zone was introduced as a second synthesis step after the solid-state reaction to produce single crystals of $Li_{0.27}La_{0.59}TiO_3$[48] and monocrystalline fibers of $Li_{0.5}La_{0.5}TiO_3$[85] to study anisotropic conductivity and the phase diagram under directional solidification, respectively.

4. Structural Characterizations of LLT

Various solid-state techniques came in aid of the researchers for characterizing this family of materials. The evolution of the structure and its dependence on the composition (Li/La ratio), substitution (A site, B site, or both), synthesis/sintering conditions, and external pressure was studied, mainly employing powder X-ray and neutron diffraction (XRD and ND), and in minor cases electron diffraction (ED). High-resolution electron microscopy (HREM) has been used to study the superstructure of LLT. Scanning electron microscopy (SEM), transmission electron microscopy (TEM), and secondary ion mass spectroscopy (SIMS) were also employed for the characterization of LLT and its related compounds.

4.1. X-ray and Neutron Powder Diffraction Study. The solid solution with the general perovskite ($CaTiO_3$)-type[98,99] formula $Li_{3x}La_{(2/3)-x}\square_{(1/3)-2x}TiO_3$ has turned out to be stable over a wide range of compositions ($\sim 0.04 < x \leq \sim 0.16$).[14,15a,32,33,42] The actual crystal structure is still controversial. In fact, depending on the amount of lattice vacancies present and the synthesis method, in addition to the simple cubic unit cell,[11,12,14,16,27,28,33,45,56,57,66,68,73,82] hexagonal,[75] tetragonal[12,14,15,29−33,35,42,44,51,59,66,68,69,73,83,87,89,100] and orthorhombic perovskite-type distorted cells[11,14−16,32,33,35,42,48,52,57,59,73,76,97] were reported. An overview of the chemical composition and crystal structure data reported for LLT in the literature is listed in Table 1.

4.1.1. Cubic Perovskite-Type Structure LLT. The cubic perovskite-type unit cell with the lattice parameter $a = 3.8$ Å (space group $Pm3m$ and $Z = 1$) was reported for a specific composition[14,27,28,33,45,68] and for samples quenched from high temperature (>1150 °C).[12,57,66,73,82] The La^{3+} ions, Li^+ ions, and vacancies are randomly distributed over the A sites. Only one work reported the identification of a double F-centered supercell with $a \approx 2a_p$ and superstructure reflections, which have been attributed to the ordering of the La^{3+} and Li^+ and vacancies at the A sites.[56] The lattice parameter a was found to decrease with increasing x in LLT (Figure 2).[57] Moreover, in the case of $Li_xLa_{0.57}TiO_3$ the lithium was found to evaporate at elevated temperature and the lattice parameter was found to increase for the $x = 0.35$

Table 1. Crystallographic Data for $Li_{3x}La_{(2/3)-x}\square_{(1/3)-2x}TiO_3$ (LLT)[a]

	lattice constant (Å)					
$x =$	a	b	c	Z	space group/crystal system	reference
0.287	3.8742(9)		7.7673(5)	1	$P4/mmm$	59
0.207	3.8717(6)		7.7850(8)	1	$P4/mmm$	59
	3.8697(8)		7.7756(5)	2	$P4/mmm$[b]	69
0.167	3.861			1	$Pm3m$	27
	12.37		4.32	10	tetragonal	31
	7.732		7.760	4	tetragonal	14
	5.374	5.374	7.600	4	$P4mm$	35
	$\sim 2a_p$	$\sim 2a_p$	$\sim 2a_p$	4	orthorhombic	68
	3.8688(4)		7.7463(2)	2	$P4/mmm$	73
	3.8703(4)			1	$Pm3m$	73
	5.4711(4)		13.404(1)	6	$R\bar{3}c$	75
0.146	3.8700(1)		7.7452(2)	2	$P4/mmm$	73
0.142	3.8673(4)		7.7528(26)	2	$P4mmm$ or $P4/mmm$	33
0.130	3.8721(1)		7.7492(4)	2	$P4/mmm$	100
0.125	7.738		7.745	8	tetragonal	14
0.117	3.8717(1)			1	$Pm3m$	33
	7.74894(3)			8	cubic	56
0.113	3.8719(2)			1	cubic	11
0.110[c]	a_p			1	$Pm3m$	66
0.110[d]	a_p		$\approx 2a_p$	2	$P4/mmm$	66
0.104	3.8727(3)		7.7510(3)	2	$P4/mmm$	73
0.100	3.8748(1)		7.7409(4)	2	$P4/mmm$	100
0.097	7.75333(3)			8	cubic	56
0.090	3.8801(3)	3.8723(3)	7.7747(6)	2	orthorhombic	48
	3.8684(1)		7.7746(1)	2	$P4/mmm$	100
0.087	3.8677(6)		7.7809(1)	1	$P4/mmm$	59
0.083	6.928	7.745	8.202	8	orthorhombic	14
0.079	3.8708(2)		7.7809(7)	2	$P4mmm$ or $P4/mmm$	33
0.073	3.8671(5)	3.8654(5)	7.7727(4)	2	$Pmmm$	73
0.070	3.8714(1)		7.7789(3)	2	$P4/mmm$	42
0.067	6.928	7.724	8.8202	8	orthorhombic	14
	7.75637(4)			2	cubic	56
0.062	3.8757(1)	3.8658(1)	7.7853(2)	2	$Pmmm$	73
0.060	3.8756(1)	3.8649(1)	7.7852(1)	2	$Pmmm$	73
	3.8757(1)	3.8655(1)	7.7845(2)	2	$Pmmm$	73
0.050	7.7313(1)	7.7520(1)	7.7840(1)	8	$Cmmm$	97
0.0417	6.916	7.732	8.195	8	orthorhombic	14
0.04	3.8747(1)	3.8632(1)	7.7846(1)	2	$Pmmm$	73
0.03	3.8753(1)	3.8638(1)	7.7901(2)	2	$Pmmm$	73

[a] a_p = cubic perovskite lattice parameter. [b] 27 °C. [c] Intermediate temperature polymorph (α), disordered phase (prepared by rapid quenching from high temperature to room temperature).[33] [d] Low-temperature polymorph (β), ordered phase (prepared by normal cooling from the elevated temperature).[33]

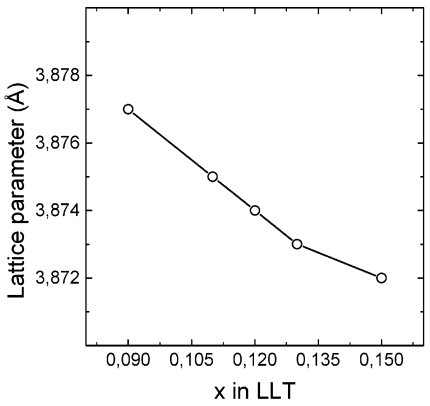

Figure 2. Variation of the cubic perovskite lattice parameter a, as a function of lithium content in $Li_{3x}La_{(2/3)-x}\square_{(1/3)-2x}TiO_3$.[57] The samples were prepared by quenching the pellets from 1350 °C into liquid nitrogen. The line passing through the data points is a guide to the eye.

and decrease for the $x = 0.30$ member with increasing sintering temperature from 1150 to 1350 °C.[82] Lithium titanium oxide and lanthanum oxide impurity phases were found to appear when the sintering time was shorter or longer than the optimum condition (6 h at 1350 °C).[16]

4.1.2. Hexagonal Perovskite-Type Structure LLT. The hexagonal unit cell has been reported for $Li_{0.5}La_{0.5}TiO_{3-\delta}$ ($0 \leq \delta \leq 0.06$) in a recent ND study,[75] the distortion being attributed to the tilting of the TiO_6 octahedra. Unit cell parameters were $a = 5.4711(4)$ Å and $c = 13.404(1)$ Å, with space group $R\bar{3}c$ ($Z = 6$), corresponding to one of Glazer's octahedral tilt schemes for perovskite-related structures,[101] which is adopted when the tilting angle of the octahedra remains small (e.g., as in the case of $LaAlO_3$, $LaCuO_3$, or $LaNiO_3$). La, Ti, and O occupy the Wyckoff position 6a site (0,0,0,25), 6b site (0,0,0), and 18e site (x,0,0.25), respectively. Difference Fourier map calculation allowed location of Li in the 18d (0.5,0,0) position.[75] The structure is constituted of nearly regular TiO_6 ochahedra (Ti−O 1.943 Å) and La is 12-fold (La−O 2.559−2.911 Å) and Li 4-fold coordination with oxygen (Figure 3). The Li ions are placed in the middle of windows, formed by four TiO_6 units, in square-planar configuration with Li−O bond lengths of 1.81−2.07 Å.

Recent investigation of $Li_{0.5}La_{0.5}TiO_3$ by means of TEM and SIMS resulted in the identification of a rigid frame, constituted of La−Ti−O, with the ordering of the La^{3+}, resulting in a superstructure where unit cell edges are doubled. The diffraction patterns of TEM mainly

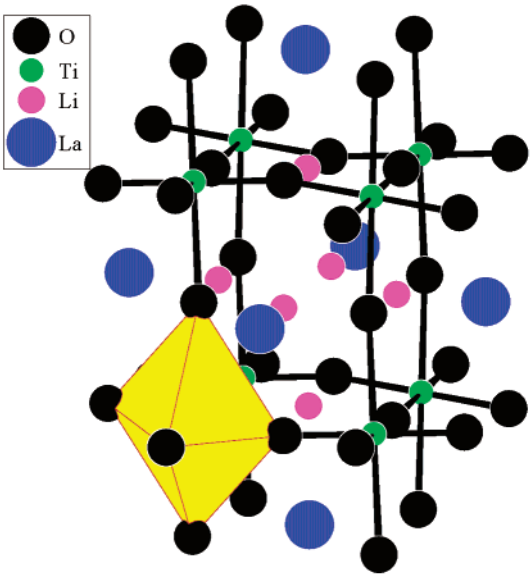

Figure 3. Schematic structure of pseudo-cubic perovskite-type $La_{0.5}Li_{0.5}TiO_3$. Ti atoms occupy the corners of the cube, oxygen atoms are at the middle of the edges, La ions (or vacancies) are the geometrical center of the cube, and Li ions are at the center of each face. The La position is half occupied; the Li position is one-sixth occupied.[75]

follow the rule for which the structure factor $F = 0$ if $(h + k + l)$ is even and $F = 0.5f_{La}$ if $(h + k + l)$ is odd, differentiating itself from the XRD response. This was attributed to the uneven distribution of La^{3+} ions at the A sites. Li_2TiO_3, as a second phase, was found at the grain boundary junctions.[68]

4.1.3. Tetragonal Perovskite-Type Structure LLT. For tetragonal phases, three types of cells have been proposed. Historically, for $Li_{0.5}La_{0.5}TiO_{3-\delta}$ ($0 \le \delta \le 0.06$),[29−31] a tungsten bronze-like[31b] cell with lattice parameters $a = 12.16$ Å and $c = 3.86$ Å[30] or $a = 12.37$ Å and $c = 4.32$ Å ($Z = 10$)[31a] has been proposed. Recent studies, employing both XRD and ND, identified two perovskite-like unit cells for $Li_{3x}La_{(2/3)-x}\square_{(1/3)-2x}TiO_3$ ($0.04 < x < 0.14$): (i) $\sqrt{2}a_p \times \sqrt{2}a_p \times c(\sim 2a_p)$ (a_p is the ideal cubic perovskite lattice parameter);[35] (ii) $a_p \times a_p \times c(\sim 2a_p)$ with space group $P4mmm$ (No. 99)[12,32,33,42,73,100] or $P4/mmm$ (No. 123).[14,66,68,69,89]

In the first case, the so-called "diagonal-distorted" unit cell was suggested by Várez et al.[35] for the $Li_{3x}La_{(2/3)-x}\square_{(1/3)-2x}TiO_{3-\delta}$ ($\sim 0.06 < x < \sim 0.16$, $0 \le \delta \le 0.06$).[32,33,42] The distortion was attributed to a 1:1 Li and La ordering along the *c*-axis, and a tilting of the TiO_6 octahedra was not excluded. This interpretation was refused by Fourquet et al.,[42] and they proposed a second type of cell on the basis of XRD and TEM studies, which has currently been accepted[12,42,44,51,59,73,83,87] (Figure 4). The TiO_6 octahedra are distorted along the *c*-axis with one short Ti−O2 (~1.8 Å) bond opposed to one long Ti−O1 (~2 Å) bond and four equal Ti−O3 (~1.94 Å) bonds.

The tetragonal distortion is attributed to the unequal distribution of vacancies, Li^+ and La^{3+} cations on the two possible crystallographic sites 1a and 1b (12-fold coordinated with oxygen) in the space group $P4/mmm$,[42] analogous to the superstructure data reported for $La_{2/3}TiO_{3-\lambda}$ ($\lambda = 0.007-0.079$).[102] This phenomenon is favored by the increase of the sintering time or of the sintering temperature above 1200 °C. The extent of the

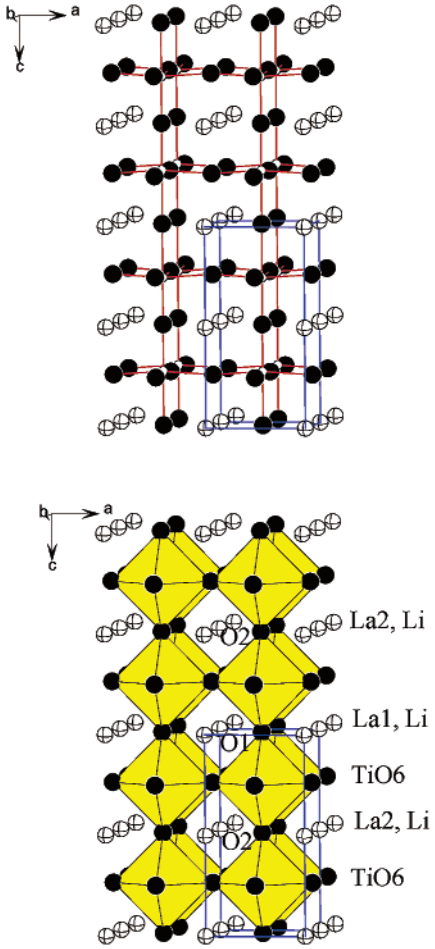

Figure 4. Crystal structure of tetragonal $Li_{3x}La_{(2/3)-x}\square_{(1/3)-2x}TiO_3$ ($x = 0.11$). (Top) ball and stick and (bottom) polyhedral view. Unit cell constant: $a = 3.8741(1)$ Å and $c = 7.7459(5)$ Å: space group $P4/mmm$.[42] The TiO_6 octahedra are connected to each other by corners.

ordered arrangements is found to increase with decreasing *x*.[14,32,55] Irregular contrast, shown by ⟨100⟩ HREM images, may be correlated to local La population fluctuations.[42] For the *x* values in the range $\sim 0.15 > x > \sim 0.04$, the tetragonal phases differ from each other only in the intensity of the superstructure reflections.[32] The tetragonal distortion $c/2a$ nearly vanishes at $x = 0.08$. Ruiz et al.[59,69] recently proposed that the actual unit formula for this compound should be doubled, $La_{1.33-x}Li_{3x}Ti_2O_6$ ($0.1 < x < 0.3$), by considering the ordering of La^{3+} ions, Li^+ ions, and vacancies. La and Li are 12-fold coordinated with oxygen.

4.1.4. Orthorhombic Perovskite-Type Structure LLT. The orthorhombic unit cell is observed mainly for a very small amount of Li ($x < 0.08$).[14,15,73,76] The distortion is generally attributed to the ordering of the A-site species (Li^+, La^{3+}, □). Two types of unit cells have been proposed: (i) $a(\sim 2a_p) \times b(\sim 2a_p) \times c(\sim 2a_p)$, where all the parameters are doubled; (ii) $a(\sim a_p) \times b(\sim a_p) \times c(\sim 2a_p)$.

In the first case, the doubling of the *c* parameter is attributed to the ordering of the vacancies along the 001 direction, while the doubling of the parameters *a* and *b* is due to the ordering of La^{3+} and Li^+ ions in the *XY*-plane [110].[14] The proposed space groups are $Cmmm$ ($x = 0.05$) (No. 65)[97a] and $Cm2m$ ($x = 0.04$) (No. 38)[97b] for

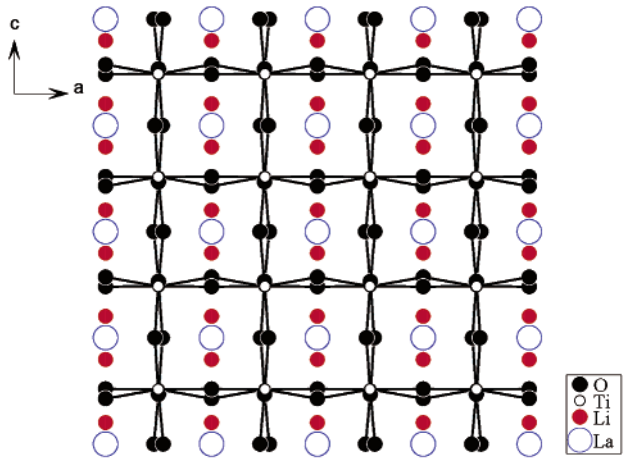

Figure 5. Crystal structure of orthorhombic $Li_{3x}La_{(2/3)-x}\square_{(1/3)-2x}TiO_3$ ($x = 0.05$). Lattice parameters: $a = 7.7313(1)$ Å; $b = 7.7520(1)$ Å, and $c = 7.7840(1)$ Å; space group $Cmmm$.[97]

the former and $Pmmm$[16] for the latter. Recent ND studies[97] support the former double cell $a(\sim 2a_p) \times b(\sim 2a_p) \times c(\sim 2a_p)$, which contains a 3D framework of corner-sharing TiO_6 octahedra that are tilted along the *b*-axis, alternatively arranged La along the *c*-axis, and Li in two equivalent off-centered positions at the A site (Figure 5). Li^+ ions are coordinated by four oxygen ions with Li−O lengths in the range 1.75−2.21 Å, which are in good agreement with the expected ones from the ionic radii after Shannon (Li(IV) = 0.59 Å and O(IV) = 1.40 Å).[103]

For the latter $a(\sim a_p) \times b(\sim a_p) \times c(\sim 2a_p)$ type, the distortion is attributed to small tilting of octahedra in the *ab*-plane or along the *c*-axis.[76] The Ti atoms are displaced from the center of the octahedral cavities toward the $z/c = 0.5$ layer, perhaps to compensate for the asymmetric distribution of charges around the octahedral site. These structural features resemble those reported by Fourquet et al.[42] and MacEachern et al.[104] The XRD analysis of single crystals indicated an orthorhombic distorted perovskite structure. Superlattice lines were attributed to the difference in the occupancy of the La(1) (0,0,0) site and the La(2) $(0,0,^1/_2)$ site accompanied by a shift of the Ti ion from the symmetric center position of the TiO_6 octahedron.[48]

5. Nuclear Magnetic Resonance (NMR) Investigations

Solid state ^{7}Li NMR is a powerful tool for studying the motion of ions. ^{7}Li is a quadrupolar nucleus ($I = {}^3/_2$), so static ^{7}Li NMR signals depend on the interactions between the electrical quadrupole moment of the Li^+ nucleus and the electric field gradient (EFG) at the site. The EFG arises as a result of the other ions surrounding the lithium ion. This makes the static spectra sensitive to changes in lattice structure and motions. Usually, the static NMR spectrum of ^{7}Li is formed by a central line, arising from the $-{}^1/_2 \leftrightarrow {}^1/_2$ transition, and by two satellites lines, coming from the ${}^1/_2 \leftrightarrow {}^3/_2$ and $-{}^1/_2 \leftrightarrow {}^3/_2$ transitions associated with the electric quadrupolar interactions.

The spin−lattice relaxation time (T_1) is a measure of the local charge-density fluctuations due to ionic motion. The dependence of the spectra and of the relaxation times T_1 (spin−lattice relaxation), T_2 (spin−spin relaxation), and $T_{1\rho}$ (spin−lattice relaxation in the rotating frame) on both temperature and composition was investigated. The magnitude of T_1 and T_2 reflects the strength of the interactions between the nuclei and their environment. Static powder pattern, with or without magic angle spinning (MAS), were recorded on $Li_{3x}La_{(2/3)-x}\square_{(1/3)-2x}TiO_3$ ($0.03 \le x \le 0.167$) samples with different crystal symmetries.[40,41,47,51,54,55,61,66,67,73,76,80,81,95]

5.1. NMR Studies on Cubic (a_p) Structure LLT. For the $x = 0.167$ cubic LLT compound, absence of satellite peaks allowed the conclusion that Li ions occupy highly symmetric sites.[40] At $T < 200$ K the line width of the spectra has been attributed mainly to Li−Li dipole interactions, while at $T > 200$ K ionic motion was identified. Analysis of $1/T_2$ and $1/T_1$ vs $1000/T$ data for $x = 0.167$ yielded an activation energy for Li motion $E_s = 0.15$ eV. Further work showed that the spin−lattice relaxation can be described by a stretched-exponential correlation function.[47] Ngai and León have demonstrated, based on their calculation from the macroscopic electrical relaxation data, that this function is the same as the microscopic ion hopping conductivity correlation function.[64,65] Therefore, the property of crystalline LLT turns out to be a special case, distinctly different from ionic glasses, which exhibit a large difference between nuclear spin relaxation and ion conductivity relaxation.[105]

5.2. NMR Studies on Tetragonal ($a_p \times a_p \times 2a_p$) Structure LLT. In tetragonal perovskites ($a = b = 3.87$ Å; $c = 2a$),[42,51,61] two kinds of Li ions exist (Figure 4 and section 4.1.3.) in different environments. One kind of Li is present in (or near) the 1a (0,0,0) site and preferentially surrounded by La^{3+}, and another kind of Li is present in (or near) the 1b (0,0,0.5) site and surrounded by either La^{3+}, other Li^+, and /or vacancies in the space group $P4/mmm$. These may explain the different mobilities recorded by NMR spectra. The spin−lattice relaxation times T_1 vs $1/T$ curves showed a strong asymmetry,[51,61] which could not be explained by an ionic motion occurring in lower dimensions (1D or 2D) as described by Richards.[106] In a first approximation, this asymmetry was explained in terms of correlated motion[107−110] and by assuming that the dynamics is governed by a distribution of activation energies for the thermally activated Li^+ ion hops.

The existence of a distribution of energy barriers is undoubtedly connected to the disorder present in these crystalline materials[110,111]and it is clearly revealed by the powder XRD analysis. The T_1 ($x = 0.11$) values[41] are comparable with those measured by Latie et al.[13] for $Li_{0.05}La_{0.33}Nb_{0.95}Ti_{0.05}O_3$. Very recently, T_1 and T_{1p} studies, performed on the ^{6}Li nucleus,[95] clearly show that just dipolar nuclear interaction is responsible for Li^+ relaxation. This result is different from that previously put forward regarding the relaxation process in these compounds.

The spin−lattice relaxation time T_1 of ^{7}Li was measured for tetragonal structure LLT ($x = 0.11$) together with cubic structure of the same position as a function of the order parameter S.[66,80] Major observations are a similar extent of the strong Li−Li correlation irrespective of S and a decrease of the uniformity of the Li sites

with increasing S. Plots of $1/T_1$ vs $1000/T$ as a function of the order parameter S show a minimum at ~70 °C, shifting very slightly to a lower temperature with decreasing S.[66] This observation roughly follows the Bloemberger−Purcell−Pound expression, which assumes isotropic, 3D motion. The magnitude of the T_1 value (~0.1 s at 250 K for $x = 0.11$) is comparable to that of León et al.[40] but it was found to be much higher compared to the Emery et al. value (4 ms at 300 K for $x = 0.08$).[51] This difference assumed due to the paramagnetic impurities in the samples.[66] However, Emery et al. related the spin−lattice relaxation (T_1) to correlation time, τ_c, of ionic motion and proposed two different natures for lithium ion motion in LLT.[51]

5.3. NMR Studies on Orthorhombic ($a_p \times a_p \times 2a_p$) Structure LLT. In orthorhombic perovskites ($a = 3.864$ Å, $b = 3.875$ Å, $c = 7.786$ Å)[73] two types of Li, with different mobility, have been ascribed to Li located in two different planes of the perovskite. The amount of Li and vacancies observed in the plane $z/c = 0.5$ is significantly higher than that in $z/c = 0$. From this fact, the mobility of Li ion should be favored in the ab-plane (2D) with respect to the perpendicular c-axis.[73] Li with low mobility, located at $z/c = 0$ planes, displays important quadrupole constants while Li with high mobility, located at $z/c = 0.5$ planes, displays small constants. The increase of Li mobility along the series $Li_{3x}La_{(2/3)-x}\square_{(1/3)-2x}TiO_3$ ($0.03 \le x \le 0.167$) is responsible for the progressive line narrowing of the central line detected in lithium NMR spectra.

6. Electrical Conductivity Relaxation (ECR) Measurements

ECR studies have been conducted to obtain information about the dynamics of the transport process in LLT.[40,47,64,65,76] It has been demonstrated that when NMR and ECR measurements are conducted in the same frequency and temperature range, the results can be correlated and the activation energies for short- and long-range motion in these perovskites can be determined.

The frequency dependence of the real part of the conductivity shows a low-frequency plateau and a crossover to power-law dependence at high frequency. This behavior is characteristic of ion hopping and can be described using Jonscher's expression[112]

$$\sigma^*(\omega) = \sigma_{dc}[1 + (j\omega/\omega_p)^n] \quad (1)$$

where σ_{dc} is the dc conductivity, ω_p is a crossover frequency, and the exponent $n \approx 0.6$ is related to the degree of correlation among moving ions.

The dispersive behavior of the conductivity in the frequency domain can be interpreted in terms of a Kohlrausch−Williams−Watts[113] (KWW) correlation function $\phi(t)$ in the time domain, which takes the form of a stretched exponential:

$$\phi(t) = \exp[-(t/\tau_\sigma)^{\beta\sigma}] \quad (2)$$

Here τ_σ is a temperature-dependent relaxation time, thermally activated with the same E_a as the dc conductivity. The temperature dependence of the dc conductivity is non-Arrhenius over the whole temperature range (160−500 K), but Arrhenius local fits can be made, giving an activation energy $E_a = 0.40$ eV at low temperature and $E_a = 0.26$ eV at high temperatures.

7. Electrical Conductivity and Electrochemical Characterization of LLT

A major role in studying the electrical properties of LLT and related materials has been performed by ac impedance spectroscopy. Different electrodes and atmospheres have been employed; however, the interpretation of the evolution of the ionic conductivity with the temperature is not unique. dc measurements allowed determination of the prevalent ionic character of the conduction, providing a value of transference number for electrons $t_e \sim 10^{-5}$. Electrochemical techniques, such as coulometric titration, galvanostatic cycling, and cyclic voltammetry, have been used to collect information about the Li intercalation and deintercalation properties and the stability of LLT in electrochemical systems.

7.1. ac Impedance Measurements. The ionic conductivity of LLT was measured by ac impedance mostly over the frequency range from 5 Hz to 13 MHz and the temperature range 150−700 K. Influence of composition, pressure, sintering, and current collectors was widely investigated. When Au or Pt are employed as electrodes, LLT shows a small bulk resistance at the high-frequency side, a large grain boundary contribution,[11,14−17,31,32,34,44,45,48,51,52,57,59,63,82,84,86] ($R_{gb} \approx 50R_b$[32] for sintered samples), and a tail in the low-frequency side, suggesting a blocking effect of the electrodes on the mobile ions (lithium) (Figure 6).[11] All the solid solutions showed a non-Debye response,[112,114−117] typical for ionic conductors, and the ac data can be interpreted by means of the Randles equivalent circuit.[118a] Moreover, it has been observed that the shape of the curves in the complex impedance plane is strongly influenced by the type of electrodes (current collectors) employed for the measurements. Figure 6b shows a typical impedance plot for LLT with reversible lithium electrodes PP/$LiClO_4$/PC using Li metal electrodes.[11] The appearance of the low-frequency intercept[118b] in this case is proof of lithium ion conduction in the perovskite-type materials.

7.2. dc Measurements. dc experiments, with Li-ion blocking Ag electrodes, were conducted both on bulk and thin film samples. Electronic conduction values in the range 5×10^{-9} to 1×10^{-8} S/cm at room temperature were reported.[11,31] The transference number (t_e)[45] of the electrons in pure LLT was found to be less than 10^{-5} at room temperature. Measurements of the lithium ion transference number t_{Li}^+ by Tubandt's method at 480 °C, following the procedure of Hladik,[119] confirmed the lithium ion conductivity and the ionic conductivity to be entirely due to the lithium ion motion ($t_{Li+} \cong 1$).[14]

7.3. Lithium Ion Conductivity of LLT. The $x \sim 0.11$ member of LLT exhibits the highest bulk lithium ion conductivity of 1×10^{-3} S/cm at room temperature. A collection of bulk lithium conductivity and the respective activation energies for LLT is given in Table 2 together with its related structure materials. Arrhenius plots for electrical conductivity shows a bend/break of the curves at higher temperature.[11] Figure 7 shows the Arrhenius plots of the ionic conductivity of LLT determined using ac impedance of polycrystalline ($x = 0.11$)

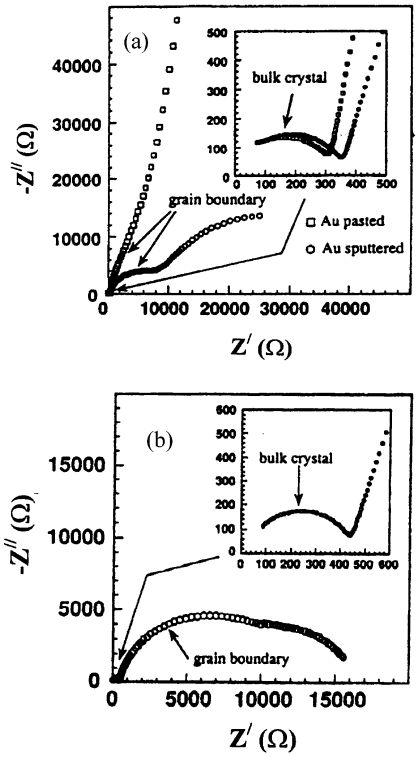

Figure 6. Typical ac impedance plots obtained in the frequency range 5 Hz to 13 MHz for $Li_{0.34}La_{0.51}\square_{0.15}TiO_{2.94}$ in air. (a) Lithium ion blocking Au pasted or sputtered electrodes at 27 °C and (b) lithium ion reversible electrodes at 17 °C. The appearance of a spike in a plot is typical for the ionic blocking behavior and absence of a tail in b indicates that the LLT is a lithium ion conductor.[11] The magnitudes of the capacitance of the bulk and grain boundary region are in the order of 100 pF and 10 nF, respectively.

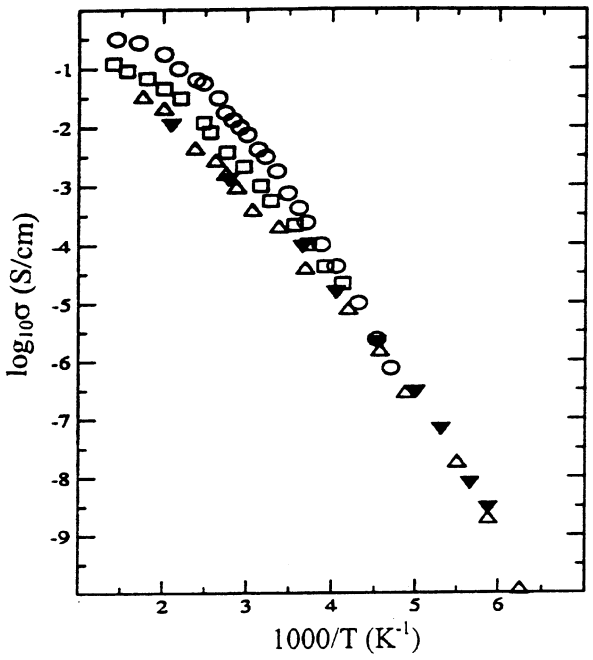

Figure 7. Arrhenius plots for lithium ion conductivity of $Li_{3x}La_{(2/3)-x}\square_{(1/3)-2x}TiO_3$ with different compositions. O: $x = 0.11$ (poly crystalline); □: $x = 0.09$ (single crystal parallel to *c*-axis);[48] △: $x = 0.06$ (dc method);[76] and ▼: $x = 0.167$ (dc method).[47]

and single crystal ($x = 0.09$) and dc method for $x = 0.06$ and 0.167 members.[11,47,48,76] At low temperature all the compounds exhibit similar conductivity values, while at higher temperature, polycrystalline materials show slightly higher conductivity than the single-crystal compound. The bending at high temperature is considered from some authors due to a phase transition, taking place at about 127 °C, which induces a conduction process with two different activation energies.[11,12,14−16,32,45,55,57,59,66,70,84] Most of the authors, anyway, describe the conduction behavior of LLT as thermally activated, like ionic conducting solid glasses[120] and define such a dependence as non-Arrhenius behavior.[40,41,44,47,48,51,61,64,65,73,76]

At higher temperature ($T > 127$ °C), conductivity data could be fitted to a Vogel−Tamman−Fulcher (VTF) type relationship,[121−123] talking then of a thermally assisted mechanism of conduction.[44] Originally, the VTF equation was developed to deal with viscosity properties of supercooled liquids[124] and it has been used to explain the temperature dependence of the ionic conductivity of polymer electrolytes.[125] The VTF behavior suggests that the mechanism of conduction involves tilting or rotating of the TiO_6 octahedra, leading to an opening and closing of the bottleneck through which the lithium ion has to move to enter an adjacent A-site vacancy, accompanied by a positive volume of activation. The bottleneck is located in the space between the two adjacent A sites, surrounded by four oxygens (in cubic lattice with space group $Pm3m$ corresponds to the 3c site, when the B-site ion occupies the 1a site) (Figure 8).[32] The temperature increase as well as the presence of more vacancies in the structure may facilitate the tilting of the octahedra, which favors a thermally assisted conduction mechanism.

The ionic conductivity is highly sensitive to the lithium content and a dome-shaped dependence of the conductivity on the Li content was observed[15a,19,20,32,39,51,57,73] (Figure 9). The effect of ionic conductivity on lithium content is discussed in section 7.5.2. The application of an external isostatic pressure[17] decreases the ionic conductivity due to lattice deformations. Thin films of the same composition of bulk materials showed a lower conductivity ($\sigma_{120°C} = 10^{-8}$–10^{-7} S/cm) with larger activation energy (1.05 eV).[49] Both conductivity and activation energy were found to be dependent on the sample preparation. dc measurements perpendicular to the surface showed high resistance, which may be due to the presence of pyrochlore $La_2Ti_2O_7$ impurity phase in the sample.[49]

7.3.1. Degree of Ordering of A-Site Cations and Vacancy. The degree of ordering of the cations and vacancies on the A sites influences strongly the crystal structure as well as lithium ion conductivity in LLT. An extensive study has been conducted by Harada and others,[12,52,57,66,70] who introduced an order parameter *S*, which is defined for alternative arrangement in the tetragonal phase, as[57]

$$S = \frac{R(\text{La-rich}) - R(\text{dis})}{1 - R(\text{dis})} \qquad (3)$$

where R(La-rich) and R(dis) are the occupancies of the A sites by La^{3+} ions in the La-rich layers of the ordered form and in the (001) plane of the disordered form, respectively. The disordered cubic form (which can be quenched from high temperatures) has a higher con-

Table 2. Bulk Lithium Ion Conductivities at 27 °C and Activation Energies of Selected LLTs and Its Related Structure Materials

compound	σ_{bulk} (S/cm)	E_a (eV)	reference
$Li_{0.34}La_{0.51}TiO_{2.94}$	1.0×10^{-3}	0.40	11
$Li_{0.27}La_{0.59}TiO_3$	6.8×10^{-4} $\perp^{c-axis}$	0.36	48
	5.8×10^{-4} $\parallel^{c-axis}$	0.35	
$Li_{0.34}La_{0.56}TiO_3$ (cubic, a_p)	1.53×10^{-3}	0.33	57
$Li_{0.34}La_{0.56}TiO_3$ (tetragonal, a_p, $2a_p$)	6.88×10^{-4}	0.35	57
$Li_{0.10}La_{0.63}TiO_3$	7.9×10^{-5}	0.36	15a
$(Li_{0.1}La_{0.5})_{0.9}Sr_{0.1}TiO_3$	1.5×10^{-3}		15a
$Li_{0.15}La_{0.51}Sr_{0.15}TiO_3$	5.3×10^{-5}	0.38	15b
$Li_{0.25}La_{0.41}Sr_{0.25}TiO_3$	7.6×10^{-5}	0.35	15b
$(Li_{0.1}La_{0.63})(Mg_{0.5}W_{0.5})O_3$	$\sim 10^{-6}$	0.39	15a
$(La_{0.5}Li_{0.5})_{1-x}(La_{0.5}Na_{0.5})_xTiO_3$ ($x > 0.4$)	$<10^{-7}$		15a
$(La_{0.5}Li_{0.5})_{1-x}(La_{0.5}Na_{0.5})_xTiO_3$ ($x = 0.25$)	2×10^{-5}		15a
$Li_{0.5}(La_{0.4}Nd_{0.1})TiO_3$	$\sim 10^{-3}$	0.33	45
$Li_{0.245}La_{0.592}Ti_{0.98}Mn_{0.02}O_3$	$\sim 10^{-3}$		58
$La_{0.58}Li_{0.36}Ti_{0.95}Mg_{0.05}O_3$	2.1×10^{-4}	0.29	78
$La_{0.56}Li_{0.36}Ti_{0.95}Al_{0.05}O_3$	6.4×10^{-4}	0.26	78
$La_{0.55}Li_{0.36}Ti_{0.95}Mn_{0.05}O_3$	1.9×10^{-4}	0.29	78
$La_{0.55}Li_{0.36}Ti_{0.95}Ge_{0.05}O_3$	3.6×10^{-4}	0.29	78
$La_{0.55}Li_{0.36}Ti_{0.95}Ru_{0.05}O_3$	5.2×10^{-5}	0.28	78
$La_{0.51}Li_{0.36}Ti_{0.95}W_{0.05}O_3$	7.3×10^{-4}	0.27	78
$La_{0.54}Li_{0.36}TiO_3$	8.9×10^{-4}	0.29	78
$La_{0.55}Li_{0.36}Ti_{0.995}Al_{0.005}O_3$	1.1×10^{-3}	0.28	78
$Li_{0.067}La_{0.64}TiO_{2.99}$	7.9×10^{-5}	0.36	91
$Li_{0.06}La_{0.66}Ti_{0.93}Al_{0.06}O_3$	1.7×10^{-6}	0.36	91
$Li_{0.10}La_{0.66}Ti_{0.90}Al_{0.10}O_3$	7.3×10^{-6}	0.35	91
$Li_{0.15}La_{0.66}Ti_{0.85}Al_{0.15}O_3$	9.6×10^{-6}	0.36	91
$Li_{0.20}La_{0.66}Ti_{0.80}Al_{0.20}O_3$	4.3×10^{-5}	0.33	91
$Li_{0.25}La_{0.66}Ti_{0.75}Al_{0.25}O_3$	7.7×10^{-5}	0.35	91
$Li_{0.30}La_{0.66}Ti_{0.70}Al_{0.30}O_3$	1.7×10^{-5}	0.33	91
$La_{(1/3)-x}Li_{3x}NbO_3$			
$x = 0.01$	4.06×10^{-6}	0.36	137
$x = 0.02$	2.33×10^{-5}	0.33	137
$x = 0.03$	3.52×10^{-5}	0.35	137
$x = 0.04$	4.25×10^{-5}	0.37	137
$x = 0.05$	3.85×10^{-5}	0.36	137
$x = 0.06$	3.82×10^{-5}	0.34	137
$La_{0.67-x}Na_{1.5x}TiO_3$			
$x = 0.08$	$<10^{-7}$	0.92	87b
$x = 0.14$	$<10^{-7}$	0.92	87b
$Li_{0.25}La_{0.25}TaO_3$	1.4×10^{-5}	0.35	136b

ductivity with a lower activation energy, $E_a = 0.33$ eV, than the ordered tetragonal phase (obtained after annealing at high temperatures), $E_a = 0.36$ eV. Cycling experiments have demonstrated that the order parameter S can be changed reversibly by annealing in a range from 600 to 1150 °C. The decrease in ionic conductivity is attributed to an increase in activation energy for ionic conduction, which is associated with the a-axis contraction in the primitive cell. The ionic conductivity decreases with increasing order parameter S (Figure 10).[12]

7.3.2. Electrochemical Characterization. Due to the very high lithium ion conductivity, LLT has been investigated with regard to its stability against lithium and intercalation of lithium using several electrochemical methods that include galvanostatic insertion,[34,38,44] coulometric titration,[25,44,50] and discharge/charge characteristics.[34,44]

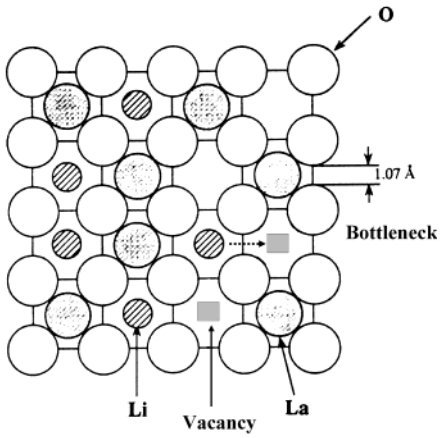

Figure 8. Schematic representation of the bottleneck for lithium ion conduction in the perovskite structure $Li_{3x}La_{(2/3)-x}\square_{(1/3)-2x}TiO_3$. Li^+, La^{2+}, and vacancy are surrounded by 12 oxygen ions. The diameter of the bottleneck is estimated to be 1.07 Å using the ideal perovskite cell, $a_p = 3.871$ Å, and the ionic radius 1.40 Å for O^{2-} ion with six coordination.[17]

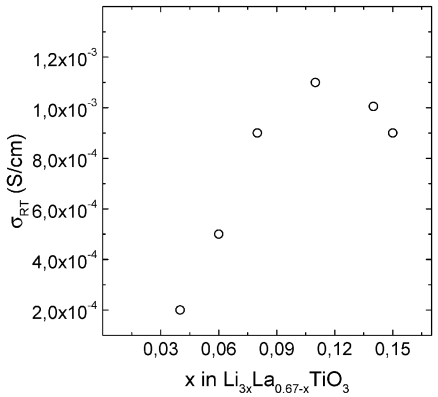

Figure 9. Variation of the lithium ion conductivity at room temperature of $Li_{3x}La_{(2/3)-x}\square_{(1/3)-2x}TiO_3$ as a function of lithium concentration. Dome-shaped behavior with a maximum at $x \approx 0.1$ is observed.[32]

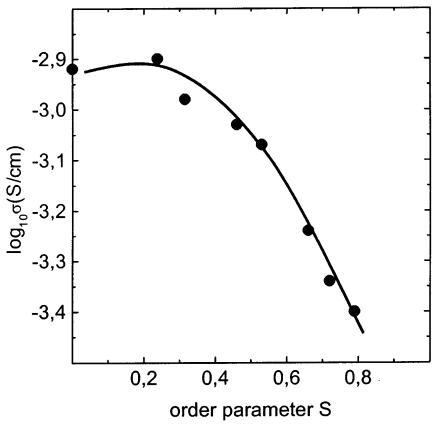

Figure 10. Bulk ionic conductivity at 25 °C for $Li_{3x}La_{(2/3)-x}\square_{(1/3)-2x}TiO_3$ ($x = 0.11$) as a function of the order parameter S.[12] The line passing through the data points is a guide to the eye.

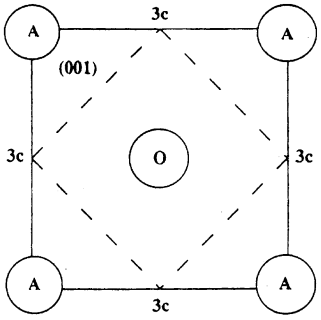

Figure 11. Schematic representation of the 001 plane of the ideal perovskite ABO_3. The solid and broken line represent the A−3c−A and 3c−3c−3c paths, respectively.[38]

The fast reduction of Ti^{4+} ions to a lower valence of 3+ by lithium insertion in A and 3c site was rationalized by the lattice self-potential, site potential, and lattice energy calculation.[34,126,127] Interestingly, lithium inserts preferably first into vacant A sites and then into interstitial 3c sites,[16,17] suggesting that occupation of A-site vacancies in the first stage of insertion is energetically favorable compared to the insertion into 3c sites.[38] The pathway of the inserted Li^+ migration can be assumed to follow two cases: (i) from an A site to a 3c site (abbreviated A−3c−A below) for the A-site deficient perovskite and (ii) from a 3c site to another 3c site (abbreviated 3c−3c−3c below) (Figure 11). The site potential at the 3c site can be assumed to take up both positive and negative values, depending on the valence of A and B. For example, for the couple $A = 0$ and $B = 6$, it has negative value. The high valence of the B cation should be advantageous for lithium insertion and conduction in the perovskite ABO_3.

Interestingly, preferential lithium insertion into interstitial sites for A site deficient perovskite oxides[128] has not been taken into account. The calculated ideal capacity was 160 mA h g^{-1}.[34] The intermittent galvanostatic discharge/charge measurement[44] showed a plateau in the discharge curve around 1.5 V vs Li/Li^+ and a maximum intercalation ratio $x = 0.15$ Li per mole of LLT. The charge curve showed that only 60% of the lithium could be extracted in this material and 50% very easily at a potential equal to the intercalation potential.

^7Li NMR experiments clearly showed that during intercalation a modification of the Li^+ ion environment takes place. The variation of the relaxation times T_1 and

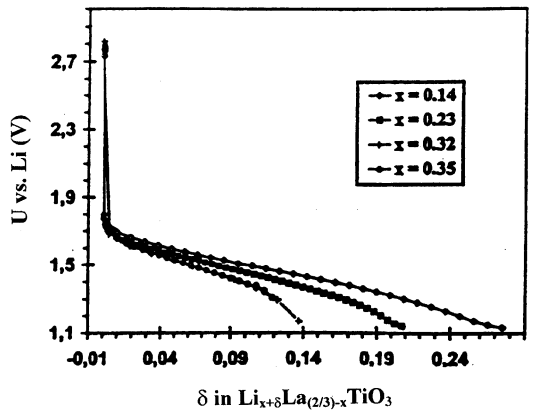

Figure 12. Coulometric titration curves of $Li_{3x}La_{(2/3)-x}\square_{(1/3)-2x}TiO_3$.[25] The measurements were performed in an electrochemical cell with a three-electrode configuration, using 1 M solution of $LiClO_4$ in PC as an electrolyte and metallic Li as counter and reference electrodes. The thickness of the LLT pellets employed for the measurements were 250−350 μm. The lines passing through the data points are guides to the eye.

T_2 of the ^7Li nuclei clearly reveals a modification of the Li^+ environment during intercalation and explained by the formation of polarons.[67,129] Two relaxation mechanisms that were observed in the ac impedance spectroscopy of the Li-intercalated samples clearly indicate the two conductive pathways for the ions and the electrons.[67,118b] For the mixed conducting sample, the electronic conductivity is predominant at low temperatures, and the ionic one becomes more and more important at high temperatures.

Coulometric titration measurements, conducted at room temperature on $Li_{x+\delta}La_{(0.66-x)}TiO_3$ samples with $x = 0.14$, 0.23, 0.32, and 0.35 showed a sharp drop of the potential from 2.8 V to 1.7 vs Li/Li^+ due to the change in the stoichiometry from $\delta = 0$ to $\delta = 1.5 \times 10^{-3}$ [25,50] (Figure 12). A contemporaneous change in color from ivory white to gray was observed. Intercalation of more Li than the expected from the number of available vacancies produced a non s-shaped titration curve, approaching a plateau attributed to the possible formation of a second phase at $\delta > 0.18$.[50] The intercalated lithium could not be fully extracted from the sample anymore in this case and the sample remained slightly gray after deintercalation.

The chemical diffusion coefficient, calculated by means of galvanostatic intermittent titration technique (GITT) theory,[130a] was estimated to be $\tilde{D} = 10^{-6}-10^{-7}$ cm^2/s for both insertion and extraction of lithium.[50] The $\tilde{D}$ values do not change markedly with respect to stoichiometric change δ. The slightly higher values of $\tilde{D}$ in the stoichiometric range $\delta = 0-0.02$ may be attributed to the comparably large number of empty lattice sites, giving more insertion paths. Furthermore, the increase of $\tilde{D}$ over both stoichiometric ranges of $\delta = 0-0.02$ and $\delta = 0.12-0.14$ may be due also to an increase of the Wagner enhancement factor, due to the increased slope of the titration curve.[130.]

7.4. Studies on Doped LLT. Chemical substitution has been carried out mainly for two purposes: (i) to improve the ionic conductivity and (ii) to stabilize the LLT against elemental Li, to use as solid electrolyte for secondary batteries. An overview of the influence of substitution on the crystal structure is given in Tables

Table 3. Crystallographic Data for A-Site Substituted $Li_{3x}La_{(2/3)-x}\square_{(1/3)-2x}TiO_3$ (LLT)[a']

chemical formula	lattice constant (Å)			Z	space group/crystal system	reference
	a	*b*	*c*			
$Li_{0.5}Nd_{0.5}TiO_3$	5.44	5.57	7.75	4	orthorhombic	29
$Li_{0.5}Nd_{0.5}TiO_3$	12.43		4.24	10	tetragonal	31
$Li_{0.5}Nd_{0.5}TiO_3$	7.652		7.672	8	tetragonal	55
β-$Li_{0.3125}Nd_{0.5625}TiO_3$	3.8245(3)		7.6809(9)	2	*P*4*mmm* or *P*4/*mmm*	33
α'-$Li_{0.3125}Nd_{0.5625}TiO_3$	5.4121(5)		7.6345(14)	8	*P*4*mmm* or *P*4/*mmm*	33
C-$Li_{0.3125}Nd_{0.5625}TiO_3$	5.4007(14)	5.4345(6)	7.6534(21)	4	*Pbnm*	33
A-$Li_{0.3125}Nd_{0.5625}TiO_3$	3.8356(2)			1	*Pm*3*m*	33
$Li_{0.34}Nd_{0.55}TiO_3$	3.8204(6)	3.823(1)	7.679(1)	2	orthorhombic	16
$Li_{0.35}Nd_{0.55}TiO_3$	5.43665(7)	7.6649(1)	5.39761(7)	4	*Pnma*	37
$Li_{0.5}Sm_{0.5}TiO_3$	5.39	5.59	7.71	4	orthorhombic	29
$Li_{0.5}Sm_{0.5}TiO_3$	5.37	5.87	7.55	4	orthorhombic	31
$Li_{0.38}Sm_{0.52}TiO_3$	5.340(3)	7.619(3)	5.441(2)	4	orthorhombic	16
$Li_{0.5}Pr_{0.5}TiO_3$	12.40		4.30	10	tetragonal	31
$Li_{0.34}Pr_{0.56}TiO_{3.01}$	3.8372(6)		7.701(1)	2	tetragonal	16
$Li_{0.38}Pr_{0.54}TiO_3$	5.43793(5)	7.66828(8)	5.40769(5)	4	*Pnma*	37
A-$Li_{0.26}Pr_{0.58}TiO_3$	3.8434(1)			1	*Pm*3*m*	43
β-$Li_{0.26}Pr_{0.58}TiO_3$	3.8332(1)		7.7226(4)	2	tetragonal	43
$Li_{0.41}Pr_{0.53}TiO_3$	5.4384(5)	7.6716(7)	5.4064(5)	4	*Pnma*	43
$Li_{0.5}Gd_{0.5}TiO_3$	5.34	5.61	7.67	4	orthorhombic	29
$Li_{0.5}Gd_{0.5}TiO_3$	5.33	5.79	7.54	4	orthorhombic	31
$Li_{0.5}Dy_{0.5}TiO_3$	5.30	5.59	7.62	4	orthorhombic	29
$Li_{0.5}Dy_{0.5}TiO_3$	5.29	5.73	7.53	4	orthorhombic	31
$Li_{0.5}Y_{0.5}TiO_3$	5.25	5.58	7.54	4	orthorhombic	29
$Li_{0.5}Y_{0.5}TiO_3$	5.28	5.73	7.52	4	orthorhombic	31
$Li_{0.5}Eu_{0.5}TiO_3$	5.36	5.88	7.55	4	orthorhombic	31
$Li_{0.5}Tb_{0.5}TiO_3$	5.32	5.74	7.55	4	orthorhombic	31
$Na_{0.5}La_{0.5}TiO_3$	3.865			1	*Pm*3*m*	27
$Na_{0.5}La_{0.5}TiO_3$	3.8734(2)			1	cubic	11
$K_{0.5}La_{0.5}TiO_3$	3.899			1	*Pm*3*m*	27
$Rb_{0.5}La_{0.5}TiO_3$	3.895			1	*Pm*3*m*	27
$Ag_{0.5}La_{0.5}TiO_3$	3.874			1	*Pm*3*m*	27
$Tl_{0.5}La_{0.5}TiO_3$	3.875			1	*Pm*3*m*	27
$(K_{0.5}La_{0.5})_xBa_{1-x}TiO_3$						
$x = 0.1$	3.999			1	cubic	30
$x = 0.2$	3.989			1	cubic	30
$x = 0.3$	3.963		4.065	1	tetragonal	30
$x = 0.5$	3.952			1	cubic	30
$x = 0.7$	3.912			1	cubic	30
$x = 0.9$	3.899			1	cubic	30
$x = 1.0$	3.894			1	cubic	30
$La_{(2/3)-x}Sr_xLi_xTiO_3$						
$x = 0.06$	5.477(6)	5.47483)	7.767(4)	4	orthorhombic	15b
$x = 0.10$	5.481(3)	5.476(2)	7.768(4)	4	othorhombic	15b
$x = 0.15$	5.489(2)	5.485(4)	7.769(3)	4	orthorhombic	15b
$x = 0.20$	5.493(4)	5.490(4)	7.771(3)	4	othorhombic	15b
$x = 0.25$	5.495(3)	5.491(1)	7.772(4)	4	othorhombic	15b
$x = 0.275$	5.497(3)	5.493(1)	7.774(3)	4	othorhombic	15b
$x = 0.30$	5.499(3)	5.494(1)	7.775(1)	4	othorhombic	15b
$(Li_{0.5}La_{0.5})_xBa_{1-x}TiO_3$						
$x = 0.2$	3.995			1	cubic	30
$x = 0.3$	3.986			1	cubic	30
$x = 0.4$	3.979			1	cubic	30
$x = 0.5$	3.975			1	cubic	30
$x = 1.0$	12.160		3.86	10	tetragonal	30
$Li_{0.33}(La_{1-x}Nd_x)_{0.56}TiO_3$						
$x = 0$	3.873			1	cubic	70
$x = 0.25$	3.863			1	cubic	70
$x = 0.5$	3.848			1	cubic	70
$x = 0.75$	3.832		7.686	2	tetragonal	70
$x = 1.0$	3.824		7.708	2	tetragonal	70
$[Ag_yLi_{1-y}]_{3x}La_{(2/3)-x}TiO_3$						
$x = 0.09$ $y = 0$	3.873(3)		7.750(8)	2	*P*4/*mmm*	87
$x = 0.09$ $y = 1/3$	3.881(2)	3.868(7)	7.791(4)	2	*Pmmm*	87
$x = 0.09$ $y = 0.5$	3.881(2)	3.868(7)	7.791(4)	2	*Pmmm*	87
$x = 0.09$ $y = 2/3$	3.882(0)	3.867(1)	7.791(4)	2	*Pmmm*	87
$x = 0.09$ $y = 1$	3.887(6)	3.887(6)	7.746(5)	2	*P*4/*mmm*	87

[a] α' indicates slightly different polymorph to α-phase.[33] β indicates low-temperature polymorph.[33] A indicates high-temperature polymorph.[33] C indicates orthorhombic distortion of the α'-phase.[33]

3 and 4. The electrical conductivity data of LLT and several A- or B-site substituted LLT related compounds are listed in Table 2.

7.4.1. Influence of A, B, or A and B Substitution on Structure and Electrical Conductivity. Taking $Li_{3x}La_{(2/3)-x}\square_{(1/3)-2x}TiO_3$ as reference composition, the sys-

Table 4. Crystallographic Data for Both A- and B- or B-Site Substituted $Li_{3x}La_{(2/3)-x}\square_{(1/3)-2x}TiO_3$ (LLT)[a']

chemical formula	lattice constant (Å)			Z	space group/crystal system	reference
	a	b	c			
$(Li_{0.1}La_{0.63})(Mg_{0.5}W_{0.5})O_3$	7.8075(20)	7.8349(20)	2 × 7.9145(15)	16	orthorhombic	15a
$Li_{0.20}La_{0.70}Ti_{0.70}Mn_{0.30}O_3$	3.8803(4)			1	cubic	58
$Li_{0.20}La_{0.767}Ti_{0.50}Mn_{0.50}O_3$	5.524(5)	5.479(5)	7.778(7)	4	orthorhombic	58
$Li_{0.20}La_{0.667}Ti_{0.80}Mn_{0.20}O_3$	3.871(4)		7.763(9)	2	tetragonal	58
$Li_{0.33}La_{0.56}M(IV)_xTi_{1-x}O_3$						
M(IV) = Zr x= 0.05	3.881			1	cubic	70
M(IV) = Zr x= 0.10	3.887			1	cubic	70
M(IV) = Hf x= 0.05	3.882			1	cubic	70
M(IV) = Hf x= 0.10	3.887			1	cubic	70
$Li_{0.36}La_{0.58}Ti_{0.95}Mg_{0.05}O_3$	3.884(7)			1	cubic	78
$Li_{0.36}La_{0.58}Ti_{0.95}Al_{0.05}O_3$	3.870(4)			1	cubic	78
$Li_{0.36}La_{0.58}Ti_{0.95}Mn_{0.05}O_3$	3.866(7)			1	cubic	78
$Li_{0.36}La_{0.58}Ti_{0.95}Ge_{0.05}O_3$	3.872(2)			1	cubic	78
$Li_{0.36}La_{0.58}Ti_{0.95}Ru_{0.05}O_3$	3.877(4)			1	cubic	78
$Li_{0.36}La_{0.58}Ti_{0.95}W_{0.05}O_3$	3.877(5)			1	cubic	78
$Li_{0.36}La_{0.58}Ti_{0.90}W_{0.10}O_3$	3.884(4)		7.770(1)	2	tetragonal	78
$Li_{0.36}La_{0.58}Ti_{0.995}Al_{0.005}O_3$	3.870(1)			1	cubic	78
$Li_{0.36}La_{0.58}Ti_{0.992}Al_{0.008}O_3$	3.868(1)			1	cubic	78
$Li_{0.36}La_{0.58}Ti_{0.995}W_{0.005}O_3$	3.880(2)			1	cubic	78
$Li_{0.36}La_{0.58}Ti_{0.995}Ta_{0.005}O_3$	3.869(2)			1	cubic	78
$Li_{0.5-3x}La_{0.5+x+y}Ti_{1-3y}Cr_{3y}O_3$						
polymorph A	3.8775(7)			1	cubic	72
polymorph C	5.497(6)	5.476(3)	7.758(8)	4	orthorhombic	72
polymorph β	3.873(1)		7.761(2)	2	tetragonal	72
$Li_{0.14}La_{2/3}Ti_{0.86}Fe_{0.14}O_3$	3.8769(1)	3.8904(2)	7.7821(3)	2	*Pmmm*	83
$Li_{0.25}La_{2/3}Ti_{0.75}Fe_{0.25}\ O_3$	3.8935(5)		7.7898(22)	2	*P4/mmm*	83
$Li_xLa_{2/3}Ti_{1-x}Al_xO_3$						
x = 0.06	5.479	5.471	7.772	4	orthorhombic	91
x = 0.1	5.478	5.469	7.761	4	orthorhombic	91
x = 0.15	5.469	5.466	7.729	4	orthorhombic	91
x = 0.2	5.465	5.463	7.729	4	orthorhombic	91
x = 0.25	5.457	5.454	7.717	4	orthorhombic	91
x = 0.30	5.454	5.450	7.715	4	orthorhombic	91
$Li_{0.20}Pr_{0.667}Ti_{0.80}Cr_{0.20}O_3$	3.8463(9)			1	cubic	60
$Li_{0.05}Pr_{0.917}Ti_{0.80}Cr_{0.20}O_3$	5.4569(8)	7.711(2)	5.446(1)	4	orthorhombic	60
$Li_{0.15}Pr_{0.75}Ti_{0.60}Cr_{0.40}O_3$	3.849(1)		7.705(2)	2	tetragonal	60
$La_{(1/3)-x}Li_{3x}NbO_3$						
x = 0	5.535(5)	5.620(9)	7.851(5)	4	orthorhombic	137
x = 0.01	5.532(6)	5.62(1)	7.844(8)	4	orthorhombic	137
x = 0.02	5.532(5)	5.613(9)	7.848(6)	4	orthorhombic	137
x = 0.03	5.529(4)	5.603(9)	7.837(5)	4	orthorhombic	137
x = 0.04	5.525(6)	5.59(1)	7.837(7)	4	orthorhombic	137
x = 0.05	5.516(7)	5.58(1)	7.833(4)	4	orthorhombic	137
x = 0.06	5.523(4)	5.579(7)	7.829(5)	4	orthorhombic	137
$Li_{0.25}Nd_{0.25}TaO_3$	3.8720		7.7300	2	tetragonal	136b
$Li_{0.25}Sm_{0.25}TaO_3$	3.8590		7.7100	2	tetragonal	136b
$Li_{0.25}Y_{0.25}TaO_3$	3.8220	3.8422	7.6540	4	orthorhombic	136b
$Li_{0.33}(Ca_{1-x}Sr_x)_{0.56}Ta_{0.56}Ti_{0.44}O_3$						
x = 0	5.487	5.381	3.857	2	orthorhombic	70
x = 0.3	3.860			1	cubic	70
x = 0.5	3.884			1	cubic	70
x = 0.8	3.912			1	cubic	70
x = 1.0	3.938			1	cubic	70
$Li_{0.33}(Ca_{1-x}Sr_x)_{0.56}Fe_{0.225}Ta_{0.775}O_3$						
x = 0	5.525	5.392	3.860	2	orthorhombic	70
x = 0.2	5.531	5.434	3.870	2	orthorhombic	70
x = 0.5	3.903			1	cubic	70
x = 0.8	3.935			1	cubic	70
x = 0.9	3.952			1	cubic	70
x = 1.0	3.961			1	cubic	70
$Li_{0.33}Sr_{0.56}M(III)_{0.225}Ta_{0.775}O_3$						
M(III) = Cr	3.948			1	cubic	70
M(III) = Co	3.978			1	cubic	70
M(III) = Ga	3.954			1	cubic	70
M(III) = Y	4.000		4.014	1	tetragonal	70
$LiCa_{1.65}Ti_{1.3}Nb_{1.7}O_9$	5.363(1)	5.464(1)	7.66283)	4	orthorhombic	77b
$LiCa_{1.65}Ti_{1.3}Ta_{1.7}O_9$	5.363(1)	5.456(1)	7.661(1)	4	orthorhombic	77b
$LiSr_{1.65}Ti_{2.15}W_{0.85}O_9$	3.911(1)			1	cubic	77b
$LiSr_{1.65}Ti_{1.3}Nb_{1.7}O_9$	3.932(1)			1	cubic	138a
$LiSr_{1.65}Ti_{1.3}Ta_{1.7}O_9$	3.932(1)			1	cubic	138a
$LiSr_{1.65}Zr_{1.3}Ta_{1.7}O_9$	4.017(1)			1	cubic	138a
$Li_{0.1}Sr_{0.8}Ti_{0.7}Nb_{0.3}O_3$	3.916(1)			1	cubic	138b
$Li_{0.3}Sr_{0.6}Ti_{0.5}Nb_{0.5}O_3$	3.925(1)			1	cubic	138b
$Li_{0.3}Sr_{0.6}Ti_{0.5}Ta_{0.5}O_3$	3.926(1)			1	cubic	138b
$Li_{0.3}Sr_{0.6}Ti_{0.45}Fe_{0.05}\ Ta_{0.5}O_3$	3.933(1)			1	cubic	138b
$Li_{0.3}Sr_{0.6}Ti_{0.40}Fe_{0.10}\ Ta_{0.5}O_3$	3.942(2)			1	cubic	138b
$Li_{0.3}Sr_{0.6}Ti_{0.35}Fe_{0.15}Ta_{0.5}O_3$	3.937(2)			1	cubic	138b
$Li_{0.3}Sr_{0.6}Ti_{0.20}Fe_{0.30}Ta_{0.5}O_3$	3.944(1)			1	cubic	138b

[a] A, C, and β: see Table 3.

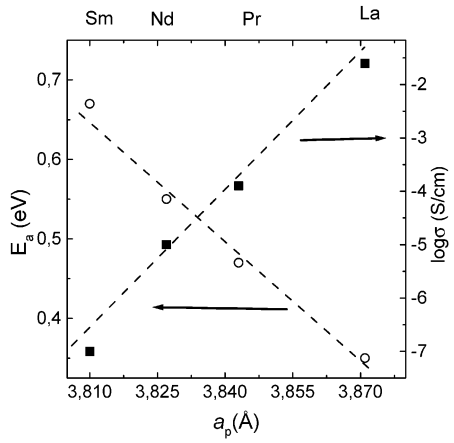

Figure 13. Variation of the ionic conductivity and the activation energy as a function of a perovskite lattice parameter for $Li_{0.34}La_{0.51}TiO_{2.94}$ (27 °C), $Li_{0.34}Pr_{0.51}TiO_{3.01}$ (27 °C), $Li_{0.34}Nd_{0.55}TiO_3$ (27 °C), and $Li_{0.38}Sm_{0.52}TiO_{2.97}$ (127 °C).[16] La compound shows the highest ionic conductivity with the lowest activation energy. The broken lines passing through the data points are guides to the eye.

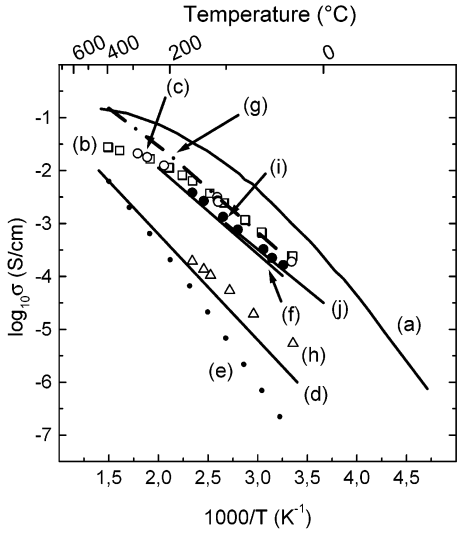

Figure 14. Arrhenius plots for electrical conductivity of (a) $Li_{0.34}La_{0.51}TiO_{2.94}$,[16] (b) $Li_{0.31}La_{0.63}Ti_{0.9}Co_{0.1}O_3$ (□),[26,96] (c) $Li_{0.31}La_{0.63}Ti_{0.9}Ni_{0.1}O_3$ (○),[26,96] (d) $Li_{0.1}La_{0.63}Mg_{0.5}W_{0.5}O_3$,[15a] (e) $Li_{0.34}Nd_{0.55}TiO_3$ (•),[16] (f) $Li_{0.1}La_{0.3}NbO_3$,[92] (g) $Li_{0.25}La_{0.25}TaO_3$ (– • –),[136b] (h) $Li_{0.3}Sr_{0.6}Nb_{0.5}Ti_{0.5}O_3$ (Δ),[138b] (i) $Li_{0.3}Sr_{0.6}Ta_{0.5}Ti_{0.5}O_3$ (●),[138b] and (j) $Li_{0.5}Sr_{0.5}Fe_{0.25}Ta_{0.75}O_3$.[70a]

tems studied in the literature can be classified as follows: (i) partial or complete substitution (Table 3) of other lanthanides (Pr, Nd, Sm, Gd, Dy, Y) for A-site La;[13,16,29,31,33,36,37,43,45,55,70,71,131,132] (ii) partial or complete substitution (Table 3) of other alkali ions Na, K, etc. or alkaline earth ions (Sr, Ba) or Ag for A-site Li;[11,15,19,20,27,30,55,74,87,129,133,134] (iii) partial or complete substitution (Table 4) of tri-, tetra-, penta-, and hexavalent ions for B-site Ti;[15,39,58,62,63,70,72,78,83,91,92,132,135−137] and (iv) contemporaneous complete substitution (Table 4) of other lanthanides or alkaline earths for A-site La and partial or complete substitution of transition metals for B-site Ti.[18,60,70,71,77,88,93,138]

In the first case, complete substitution of the La^{3+} with smaller Ln^{3+} leads to an orthorhombic distortion of the lattice, and the ionic conductivity is found to decrease accompanied by an increase in activation energy [16,31a] with decreasing ionic radius of the rare earth ion (Figure 13). Pr systems were found to show a smaller variation of the conductivity with composition compared to the La compounds.[43] Systems containing two different rare earth elements (La + Nd or La + Gd) showed two more contributions: space charge polarization and Warburg impedance at low frequencies.[45] Studies by ND have shown that the Pr and Nd compounds show a structure related to compounds such as $GdFeO_3$, $La_{1-x}TiO_3$,[104] and $(Ca,Zr)_{1-x}(LiTa)_xO_3$.[139]

In the second case, partial A-site substitution of La by monovalent alkali ions (Na, K) and divalent alkaline earth ion (Ba) did not improve much the conductivity. Indeed, Na substitution decreases the available space for Li^+ ion motion, depressing the ionic conductivity, and Ba substitution expands the lattice but induces local deformations, which decrease the ionic conductivity.[15,55] Substitution of Ag leads to a distortion of the bottlenecks that is favorable for the conduction mechanism because it decreases the activation energy.[87] Doping Sr up to 5% increases the lithium ion conduction. [12,15,19,20,52,57,70,74] It stabilizes the cubic structure and disturbs the ordering of the $Li_{0.3}La_{0.57}TiO_3$ perovskite.[74] The results indicate that ionic conductivity strongly depends on the bottleneck size, which can be modified by appropriate chemical substitution.

In the third case, it has been observed that the ionic size and amount of the substituent for Ti and the number of vacancies have a strong influence on the crystal structure and the conductivity of these materials. Larger cations and few vacancies stabilize the cubic symmetry, which indeed has been observed for Co and Ni substitution for Ti.[26,96] Interestingly, by keeping the amount of Co constant and varying the amount of vacancies, the symmetry went down to tetragonal with lattice parameters and space group similar to those proposed by Fourquet et al. for LLT.[42,96] Partial Co, Ni, and Cu substitution do not improve the ionic conductivity of LLT (Figure 14). It is interesting to point out that it is not the type of substituent but the amount of vacancies that has the major influence on the conducting behavior. Similar to LLT, doped LLT also exhibits dome-shaped dependence of the conductivity on the composition.[26,91,96]

Partial B-site substitution with Cu, Mo, and Fe for Ti induced an orthorhombic distortion.[83,96] Partial B-site substitution with Mn and Cr ($Li_{0.5-3x}La_{0.5+x+y}Ti_{1-3y}B_{3y}O_3$) showed two types of behavior depending on the amount of substituent: (i) mixed conduction with greater ionic than electronic conductivity for $0 < y \leq 0.07$ (Mn) and $0 < y \leq 0.133$ (Cr) and (ii) mixed conduction with greater electronic than ionic conductivity for $y > 0.3$ (Mn) and $y > 0.133$ (Cr). dc measurements showed that the electronic conductivity depends on the amount of Mn or Cr content in LLT.[58,72]

A small amount of Al substitution for Ti caused a very small increase in the ionic conductivity, suggesting that the change in interatomic bond strengths (both A−O and B−O bonds) is one of the factors influencing the lithium ion mobility.[78] Higher amounts of Al substitution cause a decrease in the bulk ionic conductivity by 2 orders of magnitude; for example, $Li_{0.25}La_{0.66}Ti_{0.75}Al_{0.25}O_3$ exhibits $\sigma_{bulk} = 7.6 \times 10^{-5}$ S/cm at room temperature.[91] It is expected that substitution of higher

Table 5. Room Temperature Electrical Conductivity and Activation Energy of Selected Perovskite-Type Materials without La; For Comparison, Data for $Li_{0.34}La_{0.51}TiO_{2.94}$ Are Included

compound	σ_{RT} (S/cm)	E_a (eV)	reference
$Li_{0.34}Pr_{0.56}TiO_3$	10^{-6}	0.47	16
$Sm_{0.52}Li_{0.34}TiO_3$	$<10^{-7}$	0.64	16
$Nd_{0.55}Li_{0.34}TiO_3$	$<10^{-7}$	0.53	16
$Nd_{0.25}Li_{0.25}TaO_3$	$<10^{-9}$	0.60	136b
$Sm_{0.25}Li_{0.25}TaO_3$	$<10^{-9}$	0.65	136b
$Y_{0.25}Li_{0.25}TaO_3$	$<10^{10}$	0.85	136b
$Li_{0.5}Sr_{0.56}Fe_{0.25}Ta_{0.75}O_3$	1.0×10^{-4}	0.36	70b
$Li_{0.5}Sr_{0.56}Cr_{0.25}Ta_{0.75}O_3$	6.0×10^{-5}	0.39	70b
$Li_{0.33}Sr_{0.56}Cr_{0.225}Ta_{0.775}O_3$	1.0×10^{-4}		70a
$Li_{0.33}Sr_{0.56}Co_{0.225}Ta_{0.775}O_3$	5.1×10^{-6}	0.41	70a
$Li_{0.33}Sr_{0.56}Ga_{0.225}Ta_{0.775}O_3$	7.7×10^{-6}		70a
$Li_{0.33}Ca_{0.56}Fe_{0.225}Ta_{0.775}O_3$	1.5×10^{-6}		70a
$Li_{0.33}(Ca_{0.8}Sr_{0.2})_{0.56}Fe_{0.225}Ta_{0.775}O_3$	5.8×10^{-7}		70a
$Li_{0.33}(Ca_{0.5}Sr_{0.5})_{0.56}Fe_{0.225}Ta_{0.775}O_3$	4.1×10^{-5}		70a
$Li_{0.33}(Ca_{0.2}Sr_{0.8})_{0.56}Fe_{0.225}Ta_{0.775}O_3$	9.8×10^{-5}		70a
$Li_{0.33}(Ca_{0.1}Sr_{0.9})_{0.56}Fe_{0.225}Ta_{0.775}O_3$	1.3×10^{-4}		70a
$Li_{0.33}Sr_{0.56}Fe_{0.225}Ta_{0.775}O_3$	8.5×10^{-5}		70a
$LiCaTiNbO_6$	$<10^{-7}$	0.68	138a
$LiSrTiNbO_6$	$\sim10^{-6}$	0.42	138a
$LiSrTiTaO_6$	5.5×10^{-4}	0.33	138a
$LiSr_2Ti_2NbO_9$	$<10^{-6}$	0.37	138a
$LiBa_2Ti_2NbO_9$	$<10^{-7}$	0.74	138a
$LiSr_2Ti_2TaO_9$	3.2×10^{-5}	0.27	138a
$LiCa_{1.65}Ti_{1.3}Nb_{1.7}O_9$	$<10^{-7}$	0.71	77b
$LiCa_{1.65}Ti_{1.3}Ta_{1.7}O_9$	$<10^{-7}$	0.68	77b
$LiSr_{1.65}Ti_{2.15}W_{0.85}O_9$	$\sim10^{-6}$	0.49	77b
$LiSr_{1.65}Ti_{1.3}Nb_{1.7}O_9$	2.0×10^{-5}	0.34	138a
$LiSr_{1.65}Ti_{1.3}Ta_{1.7}O_9$	4.9×10^{-5}	0.35	138a
$LiSr_{1.65}Zr_{1.3}Ta_{1.7}O_9$	1.3×10^{-5}	0.36	138a
$Li_{0.1}Sr_{0.8}Ti_{0.7}Nb_{0.3}O_3$	$\ll10^{-7}$	0.31	138b
$Li_{0.3}Sr_{0.6}Ti_{0.5}Nb_{0.5}O_3$	5.4×10^{-6}	0.31	138b
$Li_{0.3}Sr_{0.6}Ti_{0.5}Ta_{0.5}O_3$	1.7×10^{-4}	0.27	138b
$Li_{0.3}Sr_{0.6}Ti_{0.45}Fe_{0.05}Ta_{0.5}O_3$	6.0×10^{-5}	0.36	138b
$Li_{0.3}Sr_{0.6}Ti_{0.40}Fe_{0.10}Ta_{0.5}O_3$	3.6×10^{-5}	0.36	138b
$Li_{0.3}Sr_{0.6}Ti_{0.35}Fe_{0.15}Ta_{0.5}O_3$	2.8×10^{-5}	0.39	138b
$Li_{0.3}Sr_{0.6}Ti_{0.20}Fe_{0.30}Ta_{0.5}O_3$	$<10^{-7}$		138b
$Li_{0.34}La_{0.51}TiO_{2.94}$	1.0×10^{-3}	0.40	11

valence B-site ions (Nb/Ta for Ti increases the B−O bond strength, which in turn weakens the A−O bond in ABO_3 perovskites.[62] However, the substitution of Nb or Ta for Ti and K for La also does not increase the conductivity.[92] Complete substitution of the Ti by $(Mg_{0.5}W_{0.5})$ in LLT, yields a new compound, isostructural to the orthorhombic perovskite-type $La_{2/3}(Mg_{1/2}W_{1/2})O_3$,[140] which exhibits an ionic conductivity 1 order of magnitude lower compared to that of the undoped LLT ($x = 0.11$).[15]

In the last case, contemporaneous complete substitution of the La with Pr and partial B-site substitution with Cr showed mixed conduction with greater ionic than electronic conductivity for $0 < y \leq 0.10$ (y = Cr) and mixed conduction with greater electronic than ionic conductivity for $y > 0.10$.[60] Further studies on doped LLT (both A and B site) pointed out an anti-correlation between the E_a and the bulk conductivity similar to that observed in Na-β-alumina.[70,141] It must be mentioned that complete replacement of La by other rare earths or alkaline earths and partial or complete substitution of Ti by other transition metal ions do not increase the ionic conductivity (Table 5 and Figure 14).

7.5. Mechanism of Li^+ Ion Conduction. Several conduction mechanisms have been proposed for LLT on the basis of structural considerations, conductivity measurements, and theoretical models, to justify its high ionic conductivity at room temperature. Anyway, at the moment, the exact dimensionality (2D or 3D) of the lithium mobility in LLT is still controversial. Evidence of both of them is given from different experiments.

7.5.1. Structural Considerations: Vacancy, Bottleneck, and TiO_6 Octahedra Tilting. Most of the authors believe that the high ionic conductivity is due to the presence of A-site vacancies.[11,15−17,19,32,38,55,59,74,87] The exact location of Li in LLT is still not clear and many controversial results have been reported. It has been observed by means of ND study that, depending upon the composition, the structure changes its crystal symmetry and has different Li-oxygen coordination numbers. For example, the Li ions are located at the center of the A site (12-fold coordinated),[42,69] the off-center position (4-fold coordinated),[97] and the bottleneck position (4-fold coordinated)[75] for $Li_{0.32}La_{0.56}TiO_3$, $Li_{0.16}La_{0.62}TiO_3$, and $Li_{0.5}La_{0.5}TiO_3$, respectively. The highest ionic conductivity has been observed for the Li-rich compounds ($x \approx 0.10$), that is, the compounds (cubic or tetragonal perovskites) with the Li ion at the center of the A sites.

The substitution of different cations for La induces deviations in conductivity and activation energy, which have been attributed to structural randomness along the conduction paths caused by the tilting and rotating of the TiO_6 octahedra, disturbing the Li^+ ion migration.[16] Moderate lattice expansion accompanied by A-site substitution would enhance the conductivity, as observed for the substitution of up to 5% Sr for La, which was found to increase the bulk lithium ion conductivity (Table 2).[15a,19,55,74,87] However, substitution of a higher amount of Sr (>5%) for La decreases the ionic conductivity.[15] A similar effect was observed for the substitution of Ba for La,[19] which may be due to local lattice deformation caused by narrowing the bottleneck size (see section 7.3).[142,143] These observations are also applicable to other perovskite-type titanates with the general formula $M_{3x}RE_{2/3-x}TiO_3$ (where RE = rare earth element; M = Li, Na, K, Ag).[55,87] A comparative study on the pressure effect and the RE cation substitution on the ionic conductivity of the LLT showed that the former (lattice expansion) is much smaller than the latter (lattice deformation) on their ionic conductivity behavior.[17] The results have been expressed in terms of activation volume.[144]

In the cubic (disordered) and tetragonal perovskite-like structure, the Li^+ ion in the A site is surrounded by 12 oxygen ions and can migrate to the vacancy in the adjacent A site through the bottleneck surrounded by four oxygen ions (Figure 15).[17,138a,145] The positive activation volume (ΔV) value of 1.6−1.7 cm^3/mol (smaller than that of Sodium Super Ionic Conductor, NASICON, 2.8 cm^3/mol[146])[17] implies that a dilatation of the bottleneck occurs when a Li^+ ion jumps from A site to vacancy. It must be observed that due to the tilting of TiO_6 octahedra, the bottleneck is not constant all over the crystal lattice.

It has been suggested that d^0 cations such as Ti(IV), Zr(IV), Nb(V), and Ta(V) are the best choice for B cations in lithium ion conducting perovskite-type oxides[138a] because d^0 cations are known to distort BO_6 octahedra, giving rise to short and long B−O bonds.[147] A dynamic fluctuation of B−O bond lengths caused by a distorted

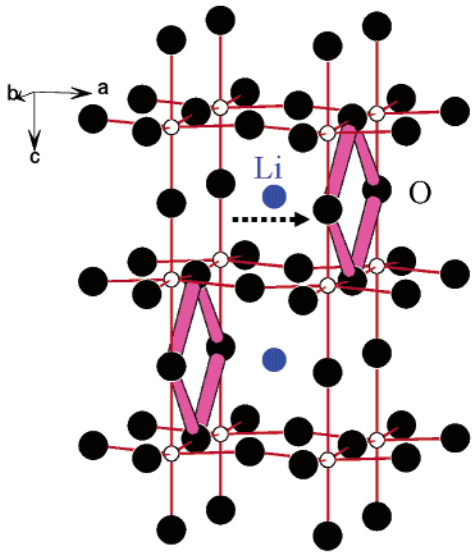

Figure 15. Schematic structure of $Li_{3x}La_{(2/3)-x}\square_{(1/3)-2x}TiO_3$ showing the bottleneck for the Li^+ ion migration. The Li, La, and vacancy are distributed at A sites.[138a]

distribution of A-site species in the perovskite structure seems to be more favorable for facile conduction than a frozen distribution of bond lengths.[138a] Since the crystal structure and conductivity changes with Li-concentration (see section, 7.5.2.), there is a lack of a single structural model to explain the conductivity behavior over the wide range of compositions in LLT.

7.5.2. Effect of Carrier Concentration and Site Percolation. For single-phase LLT the ionic conductivity is given by

$$\sigma = Z_e C \mu \tag{4}$$

where C is the concentration of the charge carriers (Li) with charge Z_e ($Z = 1$ for Li^+) and mobility μ. The mobility mainly depends on the activation energy for ionic conduction. Since the activation energy for ionic conduction is nearly constant at ambient temperature (0.35 eV), the mobility of lithium is assumed to be constant in the wide range of composition $0.06 < x < 0.15$. The charge carrier concentration involves the lithium (N_{Li}) and A-site ion vacancy (N_v) concentrations.[32] It has been assumed that all the lithium ions ($N_{Li} = 3x/V_s$) in the LLT can move independently of each other through the A-site vacancies ($N_v = (0.33 - 2x)/V_s$) for conduction. All the available A sites are presumably energetically and symmetrically equal, so one can write $N = N_{Li} + N_V$. Accordingly, the lithium ion conductivity of LLT can be expressed as[32]

$$\sigma = e\frac{(x - 6x^2)}{(0.33 + x)V_s}\mu \tag{5}$$

where V_s is the perovskite subcell volume. Reporting the value of C as a function of x, we obtain a dome-shaped curve for conductivity with a maximum at $x = 0.075$. Interestingly, the measured lithium ion conductivity as a function of x also shows the same shape[32] with a maximum at $x \approx 0.1$. Thus, the ionic conductivity of LLT does not support the hypothesis of the ordering of the A-site vacancies and cooperative ionic motion.

The highest ionic conduction in $Li_{3x}La_{(2/3)-x}\square_{(1/3)-2x}TiO_3$ was obtained when the total concentration of lithium and A-site ion vacancy $n'(0.33 + x)$ is approximately equal to 0.44−0.45. This value is higher than the site percolation threshold, n_c, value of 0.3117 for simple cubic lattice. This result suggests the presence of at least one vacancy/Li^+ adjacent to every Li^+/vacancy. The difference between the theory and experimental value is considered to be due to the local distortion. Such a distortion decreases the bottleneck and hence impedes the lithium ion jump.[19] Accordingly, the effective carrier concentration, n_{eff}, has been proposed to explain the conductivity behavior of LLT at various temperatures and is defined as[20]

$$n_{eff} \propto m(1 - m) \tag{6}$$

where m is the ratio of lithium to the sum of lithium and vacancy, $N = N_{Li} + N_V$. The conductivity can be described, using the percolation theory, by the equation[20]

$$\sigma = \frac{3x(0.33 - 2x)}{(0.33 + x)^2}\{(0.33 + x) - n_c)\} \tag{7}$$

The conductivity data measured at 227 °C is similar to that calculated using eq 7, suggesting that ionic conductivity depends on both site percolation and on the ratio of lithium to vacancy concentration.[20]

7.5.3. Theoretical Modeling. Recently, theoretical modeling of the Li-ion motion for the Li-poor composition $Li_{0.2}La_{0.6}TiO_3$ (low conducting member of LLT) has been carried out by means of molecular dynamics (MD)[148] and according to the concept of bond valence summation (BVS).[94] The MD employing the partially ionic model (PIM)[90,148] and fully ionic model (FIM)[90] could simultaneously reproduce the crystal structure and its physical properties such as thermal expansion, compressibility, and Li-ion migration. The properties, for example, density and thermal expansion coefficients obtained using PIM, were found to be close to experimental data, while the FIM model found too poor results. Both simulation and experimental data support the displacement of Li in the ⟨100⟩ direction from the center of the A site for $Li_{0.2}La_{0.6}TiO_3$. These simulations at high pressure as a function of the repulsion parameter of the Li ion, a_{Li}, reveal that the Li-ion conductivity decreases with the lattice contraction. The ionic conductivity obtained by the MD was found to be smaller than the experimental values in the temperature range 27−727 °C. For example, at 27 and 127 °C, the conductivity values from MD are 8.67×10^{-4} and 6.56×10^{-4} S/cm, while the corresponding experimental values are 1.9×10^{-4} and 4.3×10^{-3}, respectively.[90] The chemical diffusion coefficient was also found to be slightly lower than the experimental value of $Li_{0.29+\delta}La_{0.57}TiO_3$, determined by the GITT method.[50]

Mazza et al.[94] employed the BVS method, which allowed tracing to a time-averaged pathway followed by the Li^+ ion during long-range motion in the bulk of the structure. By inspection of the saddle point of such pathway, it is possible to estimate the activation energy for the ionic jump. From this calculation, the bulk conductivity could be predicted on the basis of the following three hypotheses for Li^+ ions location in the

LLT structure: (i) the Li^+ ions and vacancies are equally distributed over the La1/La2 sites,[42] (ii) all Li^+ ions are at the La2 sites, and (iii) the La2 site is completely occupied by La and Li. It has been found that the third possibility is clearly conflicting with the experimental data, while the first, redistribution of Li ion and vacancies with the same ratio on La1 and La2 sites, gives high conductivity and is comparable to the experimental values. The second possibility also produces similar results. Thus, it has been suggested that both may contribute to the conduction in LLT.

7.5.4. Analysis of NMR and ECR Data. ECR and NMR methods allowed separation of long- and short-range Li motion with distinct E_a.[44,47,51,61,67,73,76] A dispersive behavior of the conductivity, measured by ECR methods, could be interpreted both in terms of ion hopping (with correlated ion motion)[149] or of a Kohlrausch−Williams−Watts (KWW)[112] correlation function $\Phi(t)$ in the time domain.[150] NMR spin lattice relaxation results, according to Ngai's coupling model, could be evaluated giving two activation energies: E_s for long-range motion and a microscopic E_a free of the effect of cooperativity. On the basis of a thermally activated relaxation mechanism, E_s and E_a are related through the β exponent by

$$E_a = \beta_s E_s \quad [151-153] \tag{8}$$

However, it has to be pointed out that such relation between the activation energies holds only if both of them are calculated in the same temperature and frequency range.[47,154]

Ibarra et al.[73] studied the influence of composition on conductivity of these solid solutions with $0.03 \leq x \leq 0.167$. In the NMR study of orthorhombic perovskites ($a = 3.864$ Å, $b = 3.875$ Å, $c = 7.786$ Å), two types of Li, with different mobility, have been ascribed to Li located in two planes of the perovskite.[76] The accommodation of cation vacancies in alternating planes along the *c*-axis should favor a 2D movement of Li in orthorhombic samples.[59,76] However, in tetragonal samples ($a = b = 3.87$ Å; $c = 2a$), cation and vacancies turn progressively disordered, favoring a 3D movement of Li ions at higher temperature and at temperature below 200 K lithium ion hops between cages through the bottleneck in the *ab* plane (2D motion).[81,86,95] Figure 16 shows the schematic representation of 2D and 3D lithium ion mobility in LLT. This also explains the high activation energy for the low-temperature regime and low activation energy for the high-temperature region. The increase of Li mobility along the series is responsible for the progressive line narrowing of the central transition detected by ^{7}Li NMR spectra.

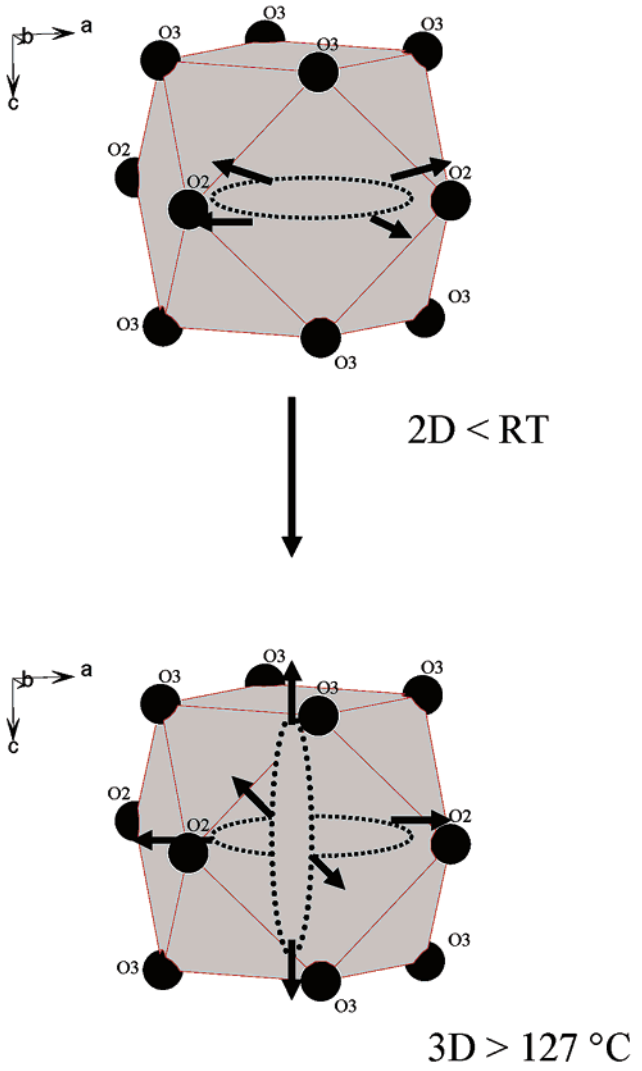

Figure 16. Schematic representation of 2D and 3D mobility of lithium ions in the perovskite structure.[86]

8. Conclusions

In summary, (i) the high lithium ionic conducting phase is the A-site defect perovskite-type $Li_{3x}La_{(2/3)-x}\square_{(1/3)-2x}TiO_3$ ($0.06 < x < 0.14$), the $x \approx 0.10$ member exhibits the highest bulk conductivity of 1×10^{-3} S/cm at 27 °C with an activation energy of ~0.40 eV. (ii) The ionic conductivity depends mainly on the size of the A-site cation, lithium ion, and vacancy concentration. LLT substituted with 5 mol % Sr for La exhibits slightly higher conductivity (1.5×10^{-3} S/cm at 27 °C) than the pure LLT, while complete substitution of other transition metal ions for Ti decreases the ionic conductivity. Complete replacement of La by other rare earth and other metal ions (alkali or alkaline earth ion) were also found to decrease the ionic conductivity. (iii) The optimum total lithium and vacancy concentration for higher ionic conductivity is found to be in the range 0.44−0.45. Lithium ion conductivity is due to the motion of lithium along the A-site vacancies, the window of four oxygens separating adjacent A sites constituting the bottleneck for lithium ion migration. (iv) Depending on the synthesis conditions and composition, LLT crystallizes in simple cubic ($a = 3.87$ Å), tetragonal ($a = b = 3.87$ Å; $c = 2a$), or orthorhombic ($a = 3.864$ Å, $b = 3.875$ Å, $c = 7.786$ Å) perovskite-type structure. Cubic structure exhibits slightly higher conductivity than the ordered tetragonal structure for the same bulk composition. The low ionic conductivity in ordered phase is due to the unequal ordering of Li, La, and vacancies along the *c*-axis. (v) NMR study reveals that at low temperature ($T >$ RT) the lithium ion hops between cages through the bottleneck in the *ab* plane, and at high temperature, the lithium ions hop in three directions.

Although LLT exhibits the highest ionic conductivity at room temperature, its use as an electrolyte is not favorable because LLT is not stable in direct contact with elemental lithium and undergoes easy and fast Li insertion with consequent reduction of Ti^{4+} to Ti^{3+}, leading to high electronic conductivity. Furthermore, the use as a lithium battery electrode is also limited because of very small lithium uptake and its practical capacity is much smaller. It is worth mentioning that LLT finds application at room temperature as a separator for selective recovery and isotope separation of lithium ion by electrolysis[21] and as pH sensors.[155] In contrast to oxide ion conductivity in ABO_3 perovskite oxides, the development of fast cation conductors, for example, Li^+ and Na^+ ion in the perovskite structure with appropriate properties for possible application in all-solid-state batteries still remains a challenge.

Acknowledgment. Dr. V. Thangadurai would like to thank the Deutscher Akademischer Austausch Dienst (DAAD), Bonn, Germany, for financial support.

References

(1) Robertson, A. D.; West, A. R.; Ritchie, A. G. *Solid State Ionics* **1997**, *104*, 1.
(2) (a) Adachi, G.-Ya; Imanaka, N.; Aono, H. *Adv. Mater.* **1996**, *8*, 127. (b) Gopalakrishnan, J.; Shukla, A. K.; Thangadurai, V. *Curr. Sci.* **1999**, *76*, 1473.
(3) Kvist, A.; Lunden, A. *Z. Naturforsch.* **1965**, *20a*, 235.
(4) West, A. R. *J. Appl. Electrochem.* **1973**, *3*, 327.
(5) (a) Hong, H. Y.-P. *Mater. Res. Bull.* **1978**, *13*, 117. (b) Bruce, P. G.; West, A. R. *Mater. Res. Bull.* **1980**, *15*, 117.
(6) (a) Kuwano, J.; West, A. R. *Mater. Res. Bull.* **1980**, *15*, 1661. (b) Alpen, V.u.; Bell, M. F.; Wichelhaus, W. *Electrochim. Acta* **1978**, *23*, 1395. (c) Rodger, A. R.; Kuwano, J.; West A. R. *Solid State Ionics* **1985**, *15*, 185.
(7) Boukamp, B. A.; Huggins, R. A. *Phys. Lett. A* **1976**, *56*, 231.
(8) Alpen, U.v.; Rabenau, A.; Talat, G. H. *Appl. Phys. Lett.* **1977**, *30*, 621.
(9) (a) Yao, Y. F. Y.; Kummer, J. T. *J. Inorg. Nucl. Chem.* **1967**, *29*, 2453. (b) Whittingham, M. S.; Huggins, R. A. *Solid State Chemistry, Mater. Bur. Stand. Spec.*; Pub. 364; U.S. GPO: Washington D.C., 1972.
(10) Aono, H.; Sugimoto, E.; Sadaoka, Y.; Imanaka, N.; Adachi, G. *J. Electrochem. Soc.* **1989**, *136*, L590.
(11) Inaguma, Y.; Liquan, C.; Itoh, M.; Nakamura, T.; Uchida, T.; Ikuta, H.; Wakihara, M. *Solid State Commun.* **1993**, *86*, 689.
(12) Harada, Y.; Hirakoso, Y.; Kawai, H.; Kuwano, J. *Solid State Ionics* **1999**, *121*, 245.
(13) Latie, L.; Villeneuve, G.; Conte, D.; Le Flem, G. *J. Solid State Chem.* **1984**, *52*, 293.
(14) Belous, A. G.; Novitskaya, G. N.; Polyanetskaya, S. V.; Gornikov, Yu. I. *Inorg. Mater.* **1987**, *23*, 412.
(15) (a) Inaguma, Y.; Chen, L.; Itoh, M.; Nakamura, T. *Solid State Ionics* **1994**, *70/71*, 196. (b) Orrantia, A. M.; Martin, S. G.; Alario-Franco, M. A. *Chem. Mater.* **2003**, *15*, 363.
(16) Itoh, M.; Inaguma, Y.; Jung, W.-H.; Chen, L.; Nakamura, T. *Solid State Ionics* **1994**, *70/71*, 203.
(17) Inaguma, Y.; Yu, J.; Shan, Y.-J.; Itoh, M.; Nakamura, T. *J. Electrochem. Soc.* **1995**, *142*, L8.
(18) Inaguma, Y.; Matsui, Y.; Shan, Y.-J.; Itoh, M.; Nakamura, T. *Solid State Ionics* **1995**, *79*, 91.
(19) Katsumata, T.; Matsui, Y.; Inaguma, Y.; Itoh, M. *Solid State Ionics* **1996**, *86*−*88*, 165.
(20) Inaguma, Y.; Itoh, M. *Solid State Ionics* **1996**, *86*−*88*, 257.
(21) Kunugi, S.; Inaguma, Y.; Itoh, M. *Solid State Ionics* **1999**, 122, 35.
(22) Klingler, M. Entwicklung neuartiger elektrochromer 3 Schicht Systeme durch insitu Erzeugung lokaler Inhomogeneitaeten in Halbleitern mittels elektrischer Spannungen, Ph.D. Thesis, Technische Fakultaet der Christian-Albrechts-Universität zu Kiel, Germany, April 1998.
(23) Klingler, M.; Chu, W. F.; Weppner, W. *Ionics* **1995**, *1*, 251.
(24) Klingler, M.; Chu, W. F.; Weppner, W. In *Extended Abstracts of the 11th International Conference on Solid State Ionics*, Honolulu, Hawaii, Nov 1997; Liebert, B. E., Weppner, W., Eds.; International Society for Solid State Ionics: Garmisch-Partenkirchen, Germany, 1997; p 431.
(25) Klingler, M.; Chu, W. F.; Weppner, W. *Ionics* **1997**, *3*, 289.
(26) Stramare, S.; Weppner, W. *Ionics* **1999**, *5*, 405.
(27) (a) Bhalla, A. S.; Guo, R.; Roy, R. *Mater. Res. Innovat.* **2000**, *4*, 3. (b) Brous, J.; Fankuchen, I.; Banks, E. *Acta Crystallogr.* **1953**, *6*, 67.
(28) Patil, P. V.; Chincholkar, V. S. *Curr. Sci.* **1970**, *39*, 348.
(29) Patil, P. V.; Chincholkar, V. S. *Indian J. Chem.* **1978**, *16*, 161.
(30) Varaprasad, A. M.; Shashi Mohan, A. L.; Chakrabarty, D. K.; Biswas, A. B. *J. Phys. C: Solid State Phys.* **1979**, *12*, 465.
(31) (a) Kochergina, L. L.; Khakhin, N. B.; Porotnikov, N. V.; Petrov, K. I. *Russ. J. Inorg. Chem.* **1984**, *29*, 506. (b) Magneli, A. *Arkiv. Kemi* **1949**, *1*, 213; **1949**, *1*, 269.
(32) Kawai, H.; Kuwano, J. *J. Electrochem. Soc.* **1994**, *141*, L78.
(33) Robertson, A. D.; Garcia Martin, S.; Coats, A.; West, A. R. *J. Mater. Chem.* **1995**, *5*, 1405.
(34) Shan, Y. J.; Chen, L.; Inaguma, Y.; Itoh, M.; Nakamura, T. *J. Power Sources* **1995**, *54*, 397.
(35) Várez, A.; Garcia-Alvarado, F.; Morán, E.; Alario-Franco, M. A. *J. Solid State Chem.* **1995**, *118*, 78.
(36) Kawai, H.; Kuwano, J. *Ceramics: Charting the Future, Advances in Science and Technology, Part 3, Proceedings of the 8th Cimtec World Ceramic Congress*, Florence, Italy; Vincenzini, P., Ed.; Techna: Faenza, Italy, 1995; p 2641.
(37) Skakle, J. M. S.; Mather, G. C.; Morales, M.; Smith, R. I.; West, A. R. *J. Mater. Chem.* **1995**, *5*, 1807.
(38) Shan, Y. J.; Inaguma, Y.; Itoh, M. *Solid State Ionics* **1995**, *79*, 245.
(39) Belous, A. G. *Solid State Ionics* **1996**, *90*, 193.
(40) León, C.; Lucía, M. L.; Santamaría, J.; Paris, M. A.; Sanz, J.; Várez, A. *Phys. Rev. B* **1996**, *54*, 184.
(41) Nairn, K. M.; Forsyth, M.; Greville, M.; MacFarlane, D. R.; Smith, M. E. *Solid State Ionics* **1996**, *86*−*88*, 1397.
(42) Fourquet, J. L.; Duroy, H.; Crosnier-Lopez, M. P. *J. Solid State Chem.* **1996**, *127*, 283.
(43) Morales, M.; West, A. R. *Solid State Ionics* **1996**, *91*, 33.
(44) Bohnke, O.; Bohnke, C.; Fourquet, J. L. *Solid State Ionics* **1996**, *91*, 21.
(45) Lee, J.-S.; Yoo, K. S.; Kim, T. S.; Jung, H. J. *Solid State Ionics* **1997**, *98*, 15.
(46) Scharner, S. Untersuchungen zur Struktur, Elektrochemie und Farbe von substituirten Lithiumtitanaten fuer moegliche Anwendungen in der Elektrochromie Ph.D. Thesis, Technische Fakultaet der Christian-Albrechts-Universität zu Kiel, Germany, November 1997.
(47) León, C.; Santamaría, M. A.; Paris, M. A.; Sanz, J.; Ibarra, J.; Torres, L. M. *Phys. Rev. B* **1997**, *56*, 5302.
(48) Inaguma, Y.; Yu, J.; Katsumata, T.; Itoh, M. *J. Ceram. Soc. Jpn.: Int. Ed.* **1997**, *105*, 597.
(49) Kitaoka, K.; Kozuka, H.; Hashimoto, T.; Yoko, T. *J. Mater. Sci.* **1997**, *32*, 2063.
(50) Birke, P.; Scharner, S.; Huggins, R. A.; Weppner, W. *J. Electrochem. Soc.* **1997**, *144*, L167.
(51) Emery, J.; Buzare, J. Y.; Bohnke, O.; Fourquet, J. L. *Solid State Ionics* **1997**, *99*, 41.
(52) Harada, Y.; Kuwano, J.; Saito, Y. Abstracts of the *4th IUMRS International Conference in Asia*, Chiba, Japan; Elsevier: Amsterdam, 1997; p 706.
(53) Klingler, M.; Chu, W. F.; Weppner, W. *Ionics* **1997**, *3*, 412.
(54) León, C.; Santamaría, J.; Paris, M. A.; Sanz, J.; Ibarra, J.; Várez, A. *J. Non-Cryst. Solids* **1998**, *235*−*237*, 753.
(55) Belous, A. G. *Ionics* **1998**, *4*, 360.
(56) Duncan, F. M.; Kirk, C. A.; Skakle, J. M. S. *ISIS Experimental Report, Technical Report*; RB No 9708; Rutherford Appleton Lab., Oxfordshire, U.K., 1998.
(57) Harada, Y.; Ishigaki, T.; Kawai, H.; Kuwano, J. *Solid State Ionics* **1998**, *108*, 407.
(58) Moreno, L.; Morales, M.; Martinez-Sarrion, M. L. *J. Solid State Chem.* **1998**, *140*, 377.
(59) Ruiz, A. I.; Lopez, M. L.; Veiga, M. L.; Pico, C. *Solid State Ionics* **1998**, *112*, 291.
(60) Morales, M.; Martinez-Sarrion, M. L. *J. Mater. Chem.* **1998**, *8*, 1583.
(61) Bohnke, O.; Emery, J.; Veron, A.; Fourquet, J. L.; Buzare, J. Y.; Florian, P.; Massiot, D. *Solid State Ionics* **1998**, *109*, 25.
(62) Chung, H.-T.; Kim, J.-G.; Kim, H.-G. *Solid State Ionics* **1998**, *107*, 153.
(63) Kim, J.-G.; Kim, H.-G.; Chung, H.-T. *J. Mater. Sci. Lett.* **1999**, *18*, 493.
(64) Ngai, K. L.; León, C. *Solid State Ionics* **1999**, *125*, 81.
(65) Ngai, K. L.; León, C. *Phys. Rev. B* **1999**, *60*, 9396.
(66) Hirakoso, Y.; Harada, Y.; Kuwano, J.; Saito, Y.; Ishikawa, Y.; Eguchi, T. *Key Eng. Mater.* **1999**, *169*−*170*, 209.
(67) Emery, J.; Bohnke, O.; Fourquet, J. L.; Buzare, J. Y.; Florian, P.; Massiot, D. *J. Phys.: Condens. Matter* **1999**, *11*, 10401.
(68) Chung, H.-T.; Cheong, D.-S. *Solid State Ionics* **1999**, *120*, 197.
(69) Ruiz, A. L.; Lopez, M. L.; Veiga, M. L.; Pico, C. *J. Solid State Chem.* **1999**, *148*, 329.
(70) (a)Watanabe, H.; Kuwano, J. *J. Power Sources* **1997**, *68*, 421. (b) Harada, Y.; Watanabe, H.; Kuwano, J.; Saito, Y. *J. Power Sources* **1999**, *81*−*82*, 777.

(71) Ishikawa, Y.; Harada, Y.; Kuwano, J. *Key Eng. Mater.* **2000**, *181*−*182*, 171.
(72) Martinez-Sarrion, M. L.; Mestres, L.; Morales, M.; Herraiz, M. *J. Solid State Chem.* **2000**, 155, 280.
(73) Ibarra, J.; Várez, A.; León, C.; Santamaría, J.; Torres-Martinez, L. M.; Sanz, *J. Solid State Ionics* **2000**, *134*, 219.
(74) Wang, G. X.; Yao, P.; Bradhurst, D. H.; Dou, S. X.; Liu, H. K. *J. Mater. Sci.* **2000**, *35*, 4289.
(75) Alonso, J. A.; Sanz, J.; Santamaría, J.; León, C.; Várez, A.; Fernández-Díaz, M. T. *Angew. Chem., Int. Ed.* **2000**, *39*, 619.
(76) París, M. A.; Sanz, J.; León, C.; Santamaría, J.; Ibarra, J.; Várez, A. *Chem. Mater.* **2000**, *12*, 1694.
(77) (a) Harada, Y.; Ishikawa, Y.; Kuwano, J.; Saito, Y. *Key Eng. Mater.* **2000**, *181*−*182*, 175. (b) Sebastian, L.; Shukla, A. K.; Gopalakrishnan, J. *Proc. Indian Acad. Sci.* (*Chem. Sci.*) **2001**, *113*, 427.
(78) Thangadurai, V.; Weppner, W. *Ionics* **2000**, *6*, 70.
(79) Mizumoto, K.; Hayashi, S. *Solid State Ionics* **2000**, *127*, 241.
(80) Hirakoso, Y.; Harada, Y.; Saito, Y.; Yoshida, Y.; Kuwano, J. *Key Eng. Mater.* **2000**, *181*−*182*, 179.
(81) Emery, J.; Bohnke, O.; Badot, J. C. In *16th International Meeting Hertzian Optics and Dielectrics*, Sept 2001; Silly, G., Buzaré, J. Y., Eds.; Université du Maine: Le Mans, France, 2001.
(82) Ban, C. W.; Choi, G. M. *Solid State Ionics* **2001**, *140*, 285.
(83) Crosnier-Lopez, M. P.; Duroy, H.; Calage, Y.; Greneche, J. M.; Fourquet, J. L. *Mater. Res. Bull.* **2001**, *36*, 651.
(84) Chen, C. H.; Amine, K. *Solid State Ionics* **2001**, *144*, 51.
(85) Várez, A.; Sanjuán, M. L.; Laguna, M. A.; Peña, J. I.; Sanz, J.; de la Fuente, G. F. *J. Mater. Chem.* **2001**, *11*, 125.
(86) Bohnke, O.; Badot, J. C.; Emery, J. In *16th International Meeting Hertzian Optics and Dielectrics*, Sept 2001; Silly, G., Buzaré, J. Y., Eds.; Université du Maine: Le Mans, France, 2001.
(87) Bohnke, O.; Bohnke, C.; Ould Sid'Ahmed, J.; Crosnier-Lopez, M. P.; Duroy, H.; Le Berre, F.; Fourquet, J. L. *Chem. Mater.* **2001**, *13*, 1593.
(88) Harada, Y.; Kuwano, J.; Saito, Y. *Key Eng. Mater.* **2002**, *214*−*215*, 227.
(89) Bohnke, O.; Duroy, H.; Fourquet, J. L.; Ronchetti, S.; Mazza, D. *Solid State Ionics* **2002**, *149*, 217.
(90) Katsumata, T.; Inaguma, Y.; Itoh, M.; Kawamura, K. *Chem. Mater.* **2002**, *14*, 3930.
(91) Morata-Orrantia, A.; García-Martín, S.; Morán, E.; Alario-Franco, M. A. *Chem. Mater.* **2002**, *14*, 2871.
(92) Nakayama, M.; Ikuta, H.; Uchimoto, Y.; Wakihara, M. *J. Mater. Chem.* **2002**, *12*, 1500.
(93) Sugiura, K.; Harada, Y.; Kuwano, J. *Key Eng. Mater.* **2002**, *216*, 127.
(94) Mazza, D.; Ronchetti, S.; Bohnké, O.; Duroy, H.; Fourquet, J. L. *Solid State Ionics* **2002**, *149*, 81.
(95) Emery, J.; Bohnke, O.; Fourquet, J. L.; Buzaré, J. Y.; Florian, P.; Massiot, D. *J. Phys.: Condens. Matter* **2002**, *14*, 523.
(96) Stramare, S. Synthesis and Characterization of Substituted Lithium Lanthanum Titanates, with Possible Application in Electrochromic Systems. Ph.D. Thesis, Technische Fakultaet der Christian-Albrechts-Universität zu Kiel, Germany, April 2002.
(97) (a) Inaguma, Y.; Katsumata, T.; Itoh, M.; Morii, Y. *J. Solid State Chem.* **2002**, *166*, 67. (b) Sanz, J.; Alonso, J. A.; Varez, A.; Fernandez-Diaz, M. T. *J. Chem. Soc., Dalton. Trans.* **2002**, (7), 1406.
(98) White, J. J.; Segall, R. L.; Barry, J. C.; Hutchison, J. L. *Acta Crystallogr., Sect. B: Struct. Sci.* **1985**, *41*, 93.
(99) Kay, H. F.; Bailey, P. C. *Acta Crystallogr., Sect. A: Found. Crystallogr.* **1957**, *10*, 219.
(100) Bhuvanesh, N. S. P.; Bohnke, O.; Duroy, H.; Crosnier-Lopez, M. P.; Emery, J.; Fourquet, J. L. *Mater. Res. Bull.* **2002**, *33*, 1681.
(101) Glazer, A. M. *Acta Crystallogr., Sect. B: Struct. Sci.* **1972**, *28*, 3384.
(102) Abe, M.; Uchino, K. *Mater. Res. Bull.* **1974**, *9*, 147.
(103) Shannon, R. D. *Acta Crystallogr., Sect. A: Found. Crystallogr.* **1976**, *32*, 751.
(104) MacEachern, M. J.; Dabkowska, H.; Garret, J. D.; Amow, G.; Gong, W.; Liu, G., Greedan, J. E. *Chem. Mater.* **1994**, *6*, 2092.
(105) Ngai, K. L. *Phys. Rev. B* **1993**, *48*, 13481.
(106) Richards, P. M. *Physics of Superionic Conductors, Topics in Current Physics*; Springer-Verlag: Berlin, 1979.
(107) Ngai, K. L.; Rendell, R. W.; Jain, H. *Phys. Rev. B* **1984**, *30*, 2133.
(108) Ngai, K. L.; Martin, S. W. *Phys. Rev. B* **1989**, *40*, 10550.
(109) Ngai, K. L. *Solid State Ionics* **1993**, *61*, 345.
(110) Walstedt, R. E.; Dupree, R.; Remeika, J. P.; Rodriguez, A. *Phys. Rev. B* **1977**, *15*, 3442.
(111) Kim, K. H.; Torgeson, D. R.; Borsa, F.; Cho, J.; Martin, S. W.; Svare, I. *Solid State Ionics* **1996**, *91*, 7.
(112) (a) Jonscher, A. K. *Dielectric Relaxation in Solids*; Chelsea Dielectric Press: London, 1983; Chapter 5. (b) León, C.; Rivera, A.; Varez, A.; Sanz, J.; Santamaría, J.; Nagi, K. L. *Phy. Rev. Lett.* **2001**, 86, 1279.
(113) Kohlrausch, R. *Ann. Phys. (Leipzig)* **1847**, *72*, 393.
(114) Jonscher, A. K.; Reau, J. M. *J. Mater. Sci.* **1978**, *13*, 563.
(115) Bruce, P. G.; West, A. R.; Almomnd, D. P. *Solid State Ionics* **1982**, *7*, 57.
(116) MacDonald, J. R. *Impedance Spectroscopy, Emphasising Solid Materials and Systems*; Wiley-Interscience: New York, 1987; Chapter 2.
(117) Irvine, J. T. S.; Sinclair, D. C.; West, A. R. *Adv. Mater.* **1990**, *2*, 138.
(118) (a) Randles, J. E. B. *Discuss. Faraday Soc.* **1947**, *1*, 11. (b) Thangadurai, V.; Huggins, R. A.; Weppner, W. *J. Power Sources* **2002**, *108*, 64.
(119) Hladik, J. *Physics of the Elements (Russian Translation)*; Mir: Moscow, 1978.
(120) Kincs, J.; Martin, S. W. *Phys. Rev. Lett.* **1996**, *76*, 70.
(121) Vogel, H. *Phys. Z.* **1921**, *22*, 645.
(122) Tamman, G.; Hesse, W. *Z. Anorg. Allg. Chem.* **1926**, *156*, 245.
(123) Fulcher, G. S. *J. Am. Ceram. Soc.* **1925**, *8*, 339.
(124) Cohen, H.; Turnbull, D. *J. Chem. Phys.* **1959**, *31*, 1164.
(125) Ratner, M. A. *Polymer Electrolytes Review Part I*; Elsevier Applied Science, London, 1987.
(126) Shan, Y. J.; Chen, L.; Inaguma, Y.; Itoh, M.; Nakamura, T. *Solid State Ionics* **1994**, *70/71*, 429.
(127) Van Gool, W.; Piken, A. G. *J. Mater. Sci.* **1969**, *4*, 95.
(128) Ho, C.; Raistrick, I. D.; Huggins, R. A. *J. Electrochem. Soc.* **1980**, *127*, 343.
(129) Austin, I. G.; Mott, N. F. *Adv. Phys.* **1969**, *18*, 41.
(130) (a) Weppner, W.; Huggins, R. A *Annu. Rev. Mater. Sci.* **1978**, *8*, 269. (b) Weppner, W.; Huggins, R. A. *J. Electrochem. Soc.* **1977**, *124*, 1569.
(131) Takahashi, H.; Baba, Y.; Ezaki, K.; Okamoto, Y.; Shibata, K.; Kuroki, K.; Nakano, S. *Jpn. J. Appl. Phys.* **1991**, *30*, 2339.
(132) Inaguma, Y.; Matsui, Y.; Yu, J.; Shan, Y.; Nakamura, T.; Itoh, M. *J. Phys. Chem. Solid* **1997**, *58*, 843.
(133) Inaguma, Y.; Sohn, J.-H.; Kim, I.-S.; Itoh, M.; Nakamura, T. *J. Phys. Soc. Jpn.* **1992**, *61*, 3831.
(134) Belous, A. G. *J. Eur. Ceram. Soc.* **2001**, *21*, 1797.
(135) Nazri, G.-A.; Julien, C. *Solid State Batteries: Materials Design and Optimization*; Kluwer: Boston, 1994; p 146.
(136) (a) Mizumoto, K.; Hayashi, S. *J. Ceram. Soc. Jpn.* **1997**, *105*, 713. (b) Mizumoto, K.; Hayashi, *S. Solid State Ionics* **1999**, *116*, 263. (c) Mizumoto, K.; Hayashi, *S. Solid State Ionics* **2000**, *127*, 241.
(137) García-Martín, S.; Rojo, J. M.; Tsukamoto, H.; Morán, E.; Alario-Franco, M. A. *Solid State Ionics* **1999**, *116*, 11.
(138) (a) Thangadurai, V.; Shukla, A. K.; Gopalakrishnan, J. *Chem. Mater.* **1999**, *11*, 835. (b) Thangadurai, V.; Weppner, W. *J. Electrochem. Soc.*, in press.
(139) Smith, R. I.; West, A. R. *J. Solid State Chem.* **1994**, *108*, 29.
(140) Yao, Y. Y.; Kummer, J. T. *J. Inorg. Nucl. Chem.* **1967**, *29*, 2453.
(141) Torii, Y. *Chem. Lett.* **1979**, 1215.
(142) Stauffer, D. *Introduction to Percolation Theory*, 1st ed.; Taylor and Francis: London, 1985.
(143) Stauffer, D.; Aharomy, A. *Introduction to Percolation Theory*, 2nd ed.; Taylor and Francis, 1992.
(144) Samara, G. A. *Solid State Physics* **1984**, *38*, 1.
(145) Thangadurai, V.; Weppner, W. *Ionics* **2002**, *8*, 281.
(146) Kafalas, J. A.; Cava, R. J. *Fast Ion Transport in Solids*; Elsevier/ North-Holland: New York, 1979; p 419.
(147) Bhuvanesh, N. S. P.; Gopalakrishnan, J. *J. Mater. Chem.* **1997**, *7*, 2297.
(148) Katsumata, T.; Inaguma, Y.; Itoh, M.; Kawamura, K. *J. Ceram. Soc. Jpn.: Int. Ed.* **1999**, *107*, 615.
(149) León, C.; Lucía, M. L.; Santamaría, J. *Phys. Rev. B* **1997**, *55*, 882.
(150) León, C.; Lucía, M. L.; Santamaría, J. *Philos. Mag. B* **1997**, *75*, 629.
(151) Ngai, K. L. *Comments Solid State Phys.* **1979,** *9*, 121.
(152) Ngai, K. L. *Comments Solid State Phys.* **1980**, *9*, 141.
(153) Ngai, K. L. *Effects of Disorder on Relaxational Processes*, Springer-Verlag: Berlin, 1994.
(154) Funke, K.; Wilmer, D. *Europhys. Lett.* **1990**, *12*, 363.
(155) Bohnke, Cl.; Duroy, H.; Fourquet, J. L. *Sensors Actuators B* **2003**, *89*, 240.

CM0300516